Check for updates

Design of engineered nanoparticles for biomedical applications by computational modeling

Diego Chaparro 🆔 and Eirini Goudeli*

Engineered nanoparticles exhibit superior physicochemical, antibacterial, optical, and sensing properties compared to their bulk counterparts, rendering them attractive for biomedical applications. However, given that nanoparticle properties are sensitive to their nanostructural characteristics and their chemical stability is largely affected by physiological conditions, nanoparticle behavior can be unpredictable *in vivo*, requiring careful surface modification to ensure biocompatibility, prevent rapid aggregation, and maintain functionality under biological environments. Therefore, understanding the mechanisms of nanoparticle formation and macroscopic behavior in physiological media is essential for the development of structure–property relationships and, their rational design for biomedical applications. Computational simulations provide insight into nanoscale phenomena and nanoparticle dynamics, expediting material discovery and innovation. This review provides an overview of the process design and characterization of metallic and metal oxide nanoparticles with an emphasis on atomistic and mesoscale simulations for their application in bionanomedicine.

1 Introduction

Nanotechnology has been a growing field of research due to proven applications of novel nanomaterials in drug or gene delivery,[1] bioimaging,[2] theranostics,[3] tissue engineering,[4] and antimicrobial materials[5] to name a few. In the scale range between 1 to 100 nm, nanoparticles (NPs) possess distinct magnetization,[6] and superior catalytic,[7] optical,[8] and antibac-

Department of Chemical Engineering, The University of Melbourne, Parkville 3010, Australia. E-mail: eirini.goudeli@unimelb.edu.au

terial activity,[9] different from bulk materials owing to their high surface-to-volume ratio.[10]

The widespread implementation of engineered nanomaterials is contingent on advancing efficient and sustainable manufacturing methods that enable their synthesis at industrial scale. For example, liquid-fed flame reactors[11] are distinguished for their ability to manufacture sophisticated functional nanomaterials at scale with diverse compositions and morphologies,[12] finding applications in gas sensing, bioimaging, and nanomedicine. These reactors have been used to manufacture gas sensors for selective detection of analytes,[13] phosphors for cell bioimaging (*e.g.*, SiO$_2$-coated Y$_2$O$_3$:Tb^{3+} (ref.

Diego Chaparro received his BSc (2015) and MSc (2018) in Chemistry from the National University of Colombia. He is a PhD candidate under the supervision of Dr Eirini Goudeli at The University of Melbourne, Australia. His research focuses on the application of computational chemistry in nanomaterials, materials science, drug design and organometallic compounds.

Diego Chaparro

Eirini Goudeli (Emerging investigator) has a diploma in chemical engineering from the University of Patras, Greece (2012) and a PhD from ETH Zurich, Switzerland (2016). Since 2018, she has been a Senior Lecturer of Chemical Engineering at The University of Melbourne, Australia. Her research focuses on multiscale modeling of aerosol reactors and gas-phase synthesis of nanoparticles with energy applications.

Eirini Goudeli

14)), dental materials,[15] radioenhancers for nanotherapeutics,[16] food supplements,[17] and nanomaterials for theranostic applications, such as aggregated Nd^{3+}-doped $BiVO_4$ luminescent nanothermometers,[18] luminescent CeO_2:Eu^{3+} for real-time H_2O_2 biosensing,[19] plasmonic SiO_2-coated Au/Fe_2O_3 nanoaggregates for photothermal killing of human breast cancer cells[20] and SnO_2 breath sensors for lung cancer diagnosis.[21] Table 1 shows a list of metallic nanoparticles, as well as metal, ceramic, and mixed oxides, highlighting their key properties and potential market applications.

Despite remarkable advancements in the production of sophisticated materials through gas-phase processes, commercialization efforts have not mirrored the same pace. Notable exceptions include the successful commercialization of nanosilver (HeiQ), amine-functionalized carbon-coated cobalt nanomagnets (TurboBeads AG), and flame-made carbon-coated iron carbide nanomagnets that are polymer-decorated with affinity binders[22] for magnetic blood purification (Hemotune AG). This delay in commercialization stems from the difficulty in controlling NP characteristics during scale-up, underscoring the need for bridging the gap between academic advancements and successful commercial applications. At the same time, the broad range of materials and compositions explored experimentally is not reflected in computational nanoscience and nano-biomedicine, which typically focuses on pristine metallic nanoparticles (most commonly gold) or a few metal oxides (Table 1). In addition, toxicological concerns must be addressed before integrating engineered NPs into biomedical devices.[23] For instance, while platinum has been used in the manufacture of silicone breast implants, questions about its toxic effects remain unresolved.[24,25]

Final product properties and their macroscopic manifestations of biological, environmental, and technological interest depend on NP size, morphology, crystallinity, state of agglomeration, and surface coating, which are largely determined by the process conditions during their synthesis.[26,27] As NP size decreases, the surface-to-volume ratio increases, enhancing electrical and thermal conductivity, while variations in NP composition, such as alloying, improves thermal stability compared to monometallic counterparts.[28] Superparamagnetism is also size-dependent, resulting in high magnetization only when NPs are exposed to a magnetic field, which disappears once the field is removed. The NP shape affects superparamagnetic properties. For example, cubic $CoFe_2O_4$ NPs exhibit lower coercivity than spherical ones.[29] The composition and crystallite size in NPs play a critical role in determining magnetic properties. Metallic NPs (Fe, Ni, Co, icosahedral Au)[30] exhibit different magnetic properties from metal oxides (Fe_3O_4, CeO_2) or nanocomposites.[31] Additionally, larger crystallite sizes enhance ferrimagnetic properties of Fe_3O_4 NPs, while smaller sizes may transition from ferrimagnetic to superparamagnetic states, facilitating their use in biomedical imaging,[32,33] smart magnetic nanocarriers,[34] and hyperthermia therapy.[35]

Nanoscale characteristics can significantly affect NP plasmonic and optical properties. Variation in size and length of Au nanorods can shift the local surface plasmonic reso-

nance,[36] while bell-shaped Au nanostructures can enhance the local electromagnetic field.[37] Surface treatment can aid in controlling NP optical properties,[38] tuning their performance as imaging agents[39,40] or in photothermal or photodynamic disease therapies.[41]

In drug delivery, nanoparticle size determines cellular uptake efficiency,[117] with NPs between 10–100 nm favoring targeted drug release.[118] The NP size, surface charge, and presence of ligands on NP surfaces influence the stability of colloidal suspensions and solubility, and hence their biological availability.[119] Large particles, for example, exhibit poor solubility, and reduced toxicity but have increased tendency to aggregate.[120] Furthermore, variations in the NP size, surface chemistry, and shape significantly affect their biodistribution and pharmacokinetics, thereby altering their toxicological profiles.[121]

Computer simulations can significantly aid in material optimization and commercialization of NPs by unravelling the mechanisms that govern nanoscale interactions during synthesis and by exploring NP reactivity with the environment.[122] These tools complement and accelerate experimental NP design[123] by exploring the effect of nanoparticle characteristics on their physicochemical properties and connecting them to performance factors for biomedical applications. A key challenge in nanomaterial modelling is their multiscale nature, ranging from 10 and 15 orders of magnitude in length and time. Quantum mechanics (QM), density functional theory (DFT), classic or reactive molecular dynamics simulations (MD), mesoscale and continuum models (Fig. 1), have been commonly used to predict NP reactivity and NP macroscopic behavior in biological media.[124] Depending on the computational model, different predictions can be made at multiple scales about NP stability, cellular interactions, and drug release kinetics. QM methods can predict Gibbs energies of solvation, chemisorption, and protein–ligand interactions.[125,126] MD and coarse-grained MD (CGMD) simulations can elucidate binding affinities,[127] protein conformational changes upon NP attachment,[128,129] ligand–protein interactions for functionalized nanomaterials,[130] drug release[131] and NP interactions with lipid membrane proteins[132] or other relevant biomolecules.[133] The effect of external electromagnetic fields on biologically relevant systems can be elucidated by MD simulations, which aid in the design of stimuli-responsive nanomaterials,[134] with applications in tissue engineering and wound healing[135] or radiofrequency cancer therapies.[136] Larger length and time scale models can be used to correlate NP characteristics with the performance in end-use applications. For example, the interaction of NPs with thermal[137,138] and electric field distributions[139] can be described by finite element method, allowing for the prediction of nanomaterial performance in sensing applications or photothermal therapies. Numerical simulations[140] and computational fluid dynamics[141] can be used to link the agglomeration state of magnetic NPs with their performance in drug delivery, hyperthermia therapies, or as magnetic resonance agents.

Table 1 Properties and biomedical applications of nanoparticles

NPs	Biomedical application	NP properties
Ag	*Antibacterial activity*: Ag⁺ ions released from oxidized Ag NPs cause cell membrane damage. Used in medical devices and textile protective articles[42]	NP size and oxidation,[43] NP shape[44] and functionalization[45] affects Ag⁺ release
	Anticoagulant activity: drug-loaded Ag NPs release phenindione molecules to improve therapeutic coagulant activity[46]	Size influence drug effect as molar ratio determines optimal drug release
	Antidiabetic activity: Ag NPs can reduce blood glucose and increase insulin levels;[47] used in surgical dressings to reduce infections and promote healing in diabetic foot treatment[48]	Sub 100 nm Ag NPs should be used to optimize Ag⁺ use in surgical dressings[48]
	Bioimaging: efficient in absorbing and scattering light, used for cancer cell bioimaging[49] and biomarkers tracking;[50] Ag NP optical activity supports potential photothermal therapy[49]	Surface functionalization[51] or coatings[49,52] on Ag NPs induces important changes in optical activity
	Drug delivery: due to their stability and biocompatibility,[53] Ag NPs can cross the blood–brain barrier and deliver anti-seizure drugs[54]	Coatings on Ag NPs determine surface charges and aggregation affecting NP cytotoxicity[55]
Au	*Anticancer activity*: Au NPs can inhibit the viability of cancer cells.[56] The efficiency of anticancer drugs can be improved by conjugating in Au NPs surfaces[57–59]	Cellular uptake of drug loaded Au NPs depends on NP size, shape and surface properties[58]
	Antioxidant activity: surface chemistry of Au NPs provides protection against reactive oxygen species,[60] finding applications in Alzheimer's disease treatment[61]	Sub 20 nm Au NPs can inhibit free radicals showing superior antioxidant and hepatoprotective effects[60]
	Bioimaging: the high biocompatibility and surface plasmon properties of Au NPs allows for their use in imaging applications such as cancer diagnosis[62]	Optical activity of Au NPs is controlled by functionalization and shape modification[62]
	Biosensors: Au nanorods are used as ultrasensitive sensors based only on surface plasmon resonance, which are capable of detecting trace amounts of analytes, such as proteins and toxins[63]	Optical activity can be tuned by changing NP dimensions[36]
	Drug delivery: nanocarrier for drug, peptide, protein and gene delivery with high biocompability[64]	Negative charge on Au NPs leads to easy conjugation for multiple fragments release[64]
	Nanotherapy: deoxyribonucleic acid (DNA) conjugation of Au NPs provides DNA targeting in infectious diseases or gene malformation[65]	Increased stability and cell uptake efficiency by easy conjugation with AuNPs[65]
Cu/CuO	*Antibacterial activity*: low-cost antibacterial agents can be produced with copper-based NPs due to their ability to produce free radicals, change cell membrane integrity, and inactivate enzymes[66]	Smaller sizes and higher reactivity for some morphologies of Cu NPs increases their cytotoxicity[67]
	Biosensors: Cu-based NPs are cheap and susceptible sensors for pesticides[68] and glucose[69]	Surface charge and size distribution of Cu NPs influences their interactions[68]
Pt	*Antibacterial activity*: small (<20 nm) PtNP composites show high antibacterial activity against pathogens[70] causing cell-membrane rupture induced by their negative zeta potential[71]	Antibacterial properties depend on NP shape, size and charge.[71] Pt NPs (<3 nm) exhibit high cytotoxicity[72]
	Anticancer activity: Pt ions released from functionalized Pt NPs induce DNA damage inhibiting its replication in various cell lines of cancer.[73] Pt NPs can potentially avoid side effects of Pt-based drugs while presenting similar reactivity during chemotherapy[74]	Pt NPs show size dependent cytotoxicity in cancer treatments.[75] Pt nanoflowers act as radioenhancers in radiation therapy[76]
	Anti-inflammatory activity: Pt NPs show scavenging activity against free radicals[77] showing potential in therapies for diseases where oxidative stress is produced[78]	Versatile functionalization of Pt NPs can tune their antioxidant activity[77]
	Antifungal activity: Pt-based NPs show remarkable antifungal activity against diverse phytopathogens[79]	Spherical and oval Pt NPs with sizes 10–50 nm possess antifungal properties[79]
	Bioimaging: the excellent magnetic imaging resonance and optical activity of Pt NPs have been exploited in cancer theranostics[80]	Photosensitizers such as porphyrins on Pt NPs improve theranostic performance
	Drug delivery: multifunctional conjugated Pt NPs are able to deliver small molecules, peptides, and antibodies in cancer treatment and diagnostics[81]	Sub 30 nm Pt NPs[82] and surface PEGylation[81] increases therapeutic efficacy
	Neuroprotection: bare and conjugated Pt NPs can inhibit aggregation of toxic Aβ amyloid peptides in Alzheimer's disease by facilitating the binding of small molecules to the amyloid.[83] Biosynthesized Pt NPs possess antioxidant and neuroprotective activity, with potential application in Parkinson's disease monitoring[84] and treatment[85]	Functionalization of Pt NPs produces stronger binding affinity with Aβ which inhibits formation of toxic oligomers[83]
Ni/NiO	*Antibacterial activity*: the interaction between NiO NPs and bacteria generates reactive oxygen species that induce lipid, protein, and DNA damage[86]	Smaller NiO NPs show greater antibacterial effect in infectious microorganisms[87]
	Antifungal activity: the radical scavenging and enzyme inhibition produced from NiO NPs causes damage in bacterial and fungal strains[88]	The oxidative stress and intracellular release of Ni²⁺ likely depend on NP size
	Antioxidant activity: moderate antioxidant activity is presented in Ni and Ni-starch NPs, which can be used to develop new therapy agents[89]	Surface conjugation is possible in Ni NPs by nanocapsulation with starch[89]
	Biosensors: laser-induced graphene/Ni nanoparticle electrode for enzyme-free glucose detection[90]	High surface area NPs allows glucose response with high sensitivity and stability[90]

Table 1 (Contd.)

NPs	Biomedical application	NP properties
TiO_2	*Antibacterial activity*: owing to their high chemical stability, low cost, and strong oxidation propensity, TiO_2 NPs can be used as antibacterial agents in coatings for medical devices and clothing[91] or in orthopedic implants[92] to prevent infection	High concentration of carboxyl groups on TiO_2 promotes stronger attachment to textiles conserving photobactericidal activity[91]
	Anticancer activity: the superior photo-catalytic activity of anatase TiO_2 inhibits tumor growth under heat[93] or ultrasonic treatment[94] in chemotherapy and phototherapy[95]	Surface conjugation of TiO_2 NPs improves their performance in photothermal and photodynamic therapies[93]
	Drug delivery: the low cost, reduced toxicity, and photoactivity of small (<30 nm) TiO_2 are desired in the formulation of nanocarriers for cancer treatments[96,97]	The conjugation of Au and TiO_2 NPs forms nanocomposites with enhanced therapeutical effects[97]
	Theranostics: TiO_2-based NPs multi-functional activity (photothermal and specific cell targeting) has been used in drug resistant pancreatic tumor therapy and diagnosis[98]	Conjugation of TiO_2 NPs with Gd^{3+} forms nanocomposites which can be loaded with receptors and drugs[98]
Fe_3O_4	*Anticancer activity*: stability, biocompatibility, magnetic hyperthermia, and high specificity make iron oxide NPs appropriate for potential cancer treatments[99]	Size and morphology dependent toxicity exhibit by Fe_3O_4 NPs[100]
	Antidiabetic activity: diabetes-inducing enzyme, α-amylase, can be inhibited by Fe_3O_4 NPs that reduce the levels of glucose uptake[101]	Surface loading of drugs on Fe_3O_4 NPs produce antidiabetic effect[101]
	Biosensors: the superior magnetic activity of Fe_3O_4-based NPs has been exploited in biosensing.[102] Different coatings can be used to tune magnetic activity and improve biosensor efficiency[103]	Sub 15 nm magnetic NPs can reach difficult access regions of the body leading to identification of circulating tumor cells[102]
	Drug delivery: engineered Fe_3O_4-based NPs have been used as biodegradable nanocarriers with good tissue penetration, low toxicity, and magneto-mechanical activity[104]	The shape of Fe_3O_4 NPs influence the biodistribution of NPs in tumor tissues showing higher anti tumor activity[105]
	Tissue engineering: the magnetic Fe_3O_4 NPs have been used in tissue disease detection or tissue regeneration by cell therapy[106]	High magnetic forces are obtained at optimized sizes and compositions of nanocarriers for tissue regeneration[106]
	Theranostics: the ability of Fe_3O_4 NPs to interact with multiple biomolecules and their good magnetic resonance imaging performance make them potential theranostic agents for cancer and other pathologies[107]	High near-infrared absorption for theranostic use is observed for core-shell Fe_3O_4–CuS nanoflower composites[107]
CeO_2	*Antibacterial activity*: CeO_2 NPs exhibit antibacterial activity in three ways: they can penetrate the membrane cell and interact with enzymes and proteins, they increase toxicity by changing the intracellular pH, or they generate reactive radicals affecting the membrane[108]	Antibacterial mechanisms depend on NP size: <30 nm cellular uptake and denaturation of proteins, <50 nm toxicity in cell wall, <100 nm induction of oxidative stress[108]
	Anticancer activity: CeO_2-based NPs can interfere with enzymatic activity and cause mitochondria and DNA damage, specifically targeting cancer cells without affecting normal ones[109]	Reactive oxygen species levels can be regulated by CeO_2 NPs involved in antitumor mechanisms[109]
	Antidiabetic activity: the high antioxidant activity of CeO_2 NPs can reduce the oxidative stress which causes complications in diabetes and increases insulin levels[110]	Ce oxidation states and oxygen vacancies suggest that CeO_2 NPs surfaces influence antioxidant effects[111]
	Antifungal activity: the multidrug-resistant fungal species is a growing concern for public health. CeO_2 show promising antifungal activity[112]	Fungicidal activity is likely due to oxidative damage of cell membrane[112] generated by CeO_2 NPs surfaces
	Drug delivery: CeO_2-based NPs have good stability and biodegradability making them suitable to design effective pH-sensitive drug delivery systems in cancer or neurodegenerative disease treatment[113]	Neutral and positive surface charges of CeO_2 NPs at different pH conditions improve their multifunctional chemotherapeutic activity[113]
	Neuroprotection: the aggregation of α-syn proteins generates amyloid filaments commonly observed in neurodegenerative diseases. These amyloids may generate radical species that damage nerve cells. Hybrid CeO_2 NPs induces surface regeneration and antioxidant activity,[114] reducing toxicity after bonding to α-syn[115]	The Ce^{4+}/Ce^{3+} pair formed on the surface of core–shell CeO_2 hybrid NPs shows antioxidant features while conserving superparamagnetic properties
	Tissue regeneration: polymeric composites of CeO_2 NPs have Ce^{4+} and Ce^{3+} valence states that affect its interaction with proteins. This is important in controlling cell proliferation and adhesion in biomedical materials[116]	Surface charges and hydrophobicity in Ce^{4+} and Ce^{3+} rich regions determines cell–NP interactions[116]

This review aims to provide an overview of most recent advances in the use of computational simulations of engineered NPs in biomedical applications. Section 2 focuses on atomistic simulations that are routinely employed to explore the effect of nanoparticle characteristics, such as structure, crystallinity, and surface characteristics, on their reactivity, oxidation, dissolution, and interactions within biological environments. Such nanoscale properties and interactions are critical for optimizing drug delivery systems and approaches for developing treatments for neurodegenerative diseases. Section 3 discusses the application of mesoscale and continuum models in nano-biomedical research. These models link nanostructural characteristics of NPs with their macroscopic manifestations, including settling behavior in nanotoxicology studies and properties such as optical activity and dissolution, crucial in biomedical research. The review concludes with a Conclusions
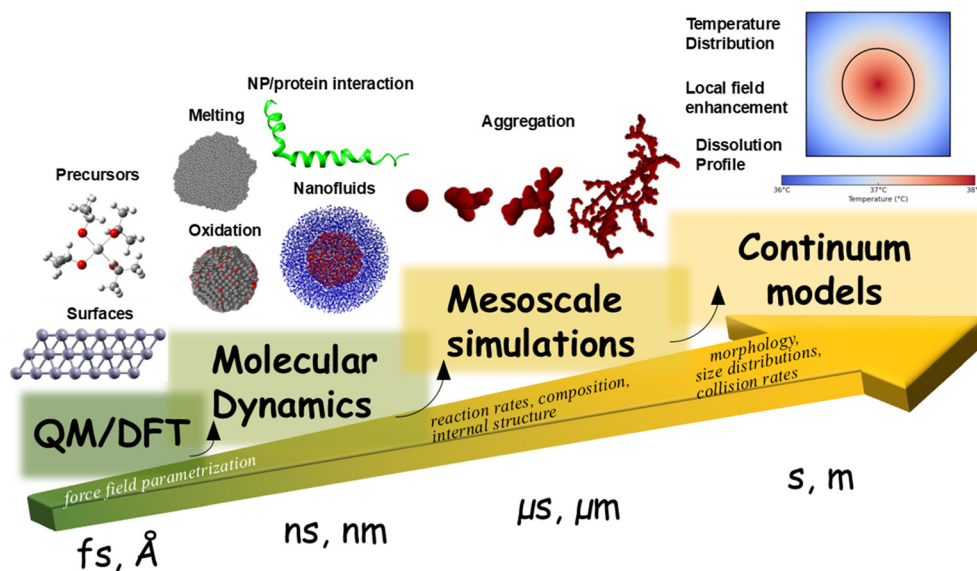
Fig. 1 Overview of time and length scales of density functional theory (DFT), molecular dynamics (MD), mesoscale, and continuum models for simulation of nanomaterials.

2 Atomistic modeling of nanoparticles: density functional theory (DFT) and molecular dynamics (MD) simulations

Assessing NP chemical stability and reactivity *in vivo* is challenging, requiring detailed understanding across multiple scales. Atomistic models are extensively used to investigate these properties at the nanosecond and nanometer scale (Fig. 1). These are instrumental in describing early stages of NP formation, growth rates, as well as their physicochemical stability and reactivity. Quantum mechanics (QM) can fully describe the electronic structure of atoms and molecules, enabling the prediction of chemical properties (*e.g.*, chemical reaction barriers, binding energies, and reaction pathways), which cannot be observed directly by experiments.[142] DFT is the most frequently applied QM approach, offering a balance between chemical accuracy and computational cost.[143] The reliability of DFT predictions depends on the selection of appropriate functionals to describe electron interactions, which must be rigorously calibrated with reference data.[144,145]

While DFT calculations focus on electronic structure which is useful for surface NP models,[146] molecular dynamics (MD) simulate the dynamic behavior and long-term interactions of NPs with water and biological media, handling up to hundreds of thousands of atoms over microsecond timeframes (Fig. 1). Classical MD has been used traditionally to model NP stability

upon their formation and growth by different mechanisms (*e.g.*, nucleation,[147] coalescence,[148] sintering[149]), phase transitions (*e.g.*, crystallization[150]), and their interactions with polymers[151] and proteins.[152] Classical force fields, however, lack the ability to model chemical reactions due to the absence of charge transfer terms and their inability to describe bond formation and breaking. To overcome this limitation, reactive force fields (FF), such as ReaxFF[153] and the charge-optimized many-body potential (COMB),[154] have been developed incorporating bond order principles from QM for the simulation of chemical reactions in a computationally feasible manner. In this section, *in silico* experiments of commonly studied metal and metal oxide NPs are discussed, highlighting the importance of their nanoscale characteristics (*e.g.*, size, crystallinity) on properties such as oxidation and dissolution rates, and thermal performance. The section then extends to more complex systems, examining interactions within biological environments by atomistic or coarse-grained simulations, emphasizing on their effect on antibacterial activity, drug-delivery capabilities and disease treatment.

2.1 Nanoparticle oxidation

The oxidation state and ion release rate are crucial in determining the antimicrobial and antibacterial NP activity.[43] The oxidation rate is affected by a range of factors, including temperature, nanomaterial purity, NP size, crystallinity, oxidation time, and oxygen concentration.[122] For example, nanosilver has remarkable antibacterial activity, finding applications in consumer products, including food containers, textiles, and cosmetics.[155,156] Even though metallic silver is not soluble in water,[157] when in the nanometer size range, it can be oxidized releasing silver ions from its surface. Such Ag^+ ion release (leaching) in aquatic environments is associated with the tox-

icity of sub-10 nm nanosilver,[158] which has been threatened with labelling as a pesticide by the US Environmental Protection Agency.[159] Combined scanning tunneling microscopy and DFT calculations[160] revealed that oxidation of (110) Ag surface (Fig. 2a) takes place by dissociation of O_2 and formation of O–Ag–O complex (Fig. 2b) that weakens the Ag–Ag bond and produces a vacancy (Fig. 2c) and a Ag adatom (Fig. 2d). The O–Ag–O complex diffuses to the closest hollow site producing a concerted motion (Fig. 2e), which induces a new vacancy (Fig. 2f). Oxidation of Ag NPs occurs by the formation of a core–shell structure, where a metallic Ag core is formed covered by a silver oxide layer.[161] The surface oxide layer predicted by reactive MD simulations thickens with decreasing nanoparticle size, consistent with ion-selective electrode experiments,[43] while sufficiently small (<2 nm) Ag NPs suffer internal oxidation.[161] An Arrhenius-type relationship describes the oxidation rate constant, showing faster oxidation at higher temperatures and lower activation energies with decreasing nanosilver size (Fig. 2g).[161] Even though the NP size plays a key role in oxidation and thus antibacterial activity of nanosilver, NP shape also affects particle oxidation. For Ag NPs with similar surface area, NP geometries with higher surface fractions of (100) and (111) facets oxidize faster compared to nanostructures with large fraction of (110) facets that are structurally less stable and lose their crystallinity more easily.[162] The influence of facets reactivity is also observed by gas–solid interfacial energy calculations for Cu[163] showing that Cu_2O monolayers can form and grow on (110) Cu facets more easily than on (100) ones, in agreement with environmental transmission electron microscopy imaging.

Likewise, platinum (Pt) is subject to rigorous scrutiny due to their potential in biomedical applications. It is used as a catalyst in the production of silicone breast implants, raising toxicological concerns associated with the residual Pt that might enter the body, either through the intact shell or in the event of implant rupture.[25] Platinum NPs have shown varying levels of toxicity, with some studies indicating cytotoxic effects through mechanisms like oxidative stress,[164] DNA damage,[165] and cell cycle arrest,[166] while others demonstrate limited harm, depending on factors such as size,[167] coating,[168] and concentration.[77] Although FDA recognizes Pt as a safe material when in its zero-oxidation state, small Pt NPs (around 1 nm) exhibit greater toxicity upon oxidation, likely due to increased Pt^{2+} ion release that disrupts DNA structures.[169] The exact mechanisms behind this varied Pt toxicity remain unclear. MD simulations using the COMB3 force field have shown that higher oxygen coverage led to destabilization of the Pt NP surface atoms.[170] Larger Pt nanoparticles, however, were more stable due to their lower surface-to-volume ratio and lower oxygen adsorption energy, making them more resistant to oxidation.

The metallic surface oxide layer that forms upon oxidation is linked not only to nanoparticle toxicity, but also to reduced performance. For example, a 0.4 nm silver oxide layer reduces surface-enhanced Raman scattering (SERS) enhancement factors by three orders of magnitude compared to unoxidized nanosilver.[171] Similarly, oxidation of Co NPs results in the formation of a Co/CoO core–shell structure, which deteriorates the overall NP magnetization due to the antiferromagnetic CoO shell dominating over the ferromagnetic Co core.[172] These experimental findings have been corroborated by DFT calculations of Co oxidation revealing the formation of a nonmagnetic Co_3O_4 layer[173] that drastically reduces NP magnetization, rendering them unsuitable for cancer theranostics.

While pure metallic NPs, such as Ag, Fe, and Cu, are susceptible to oxidation, they can achieve improved biocompatibility through surface treatment, such as coating with inert shells or functional molecules, or by combining with other materials. Such multicomponent NPs not only exhibit significantly reduced oxidation and ion release, leading to lower tox-
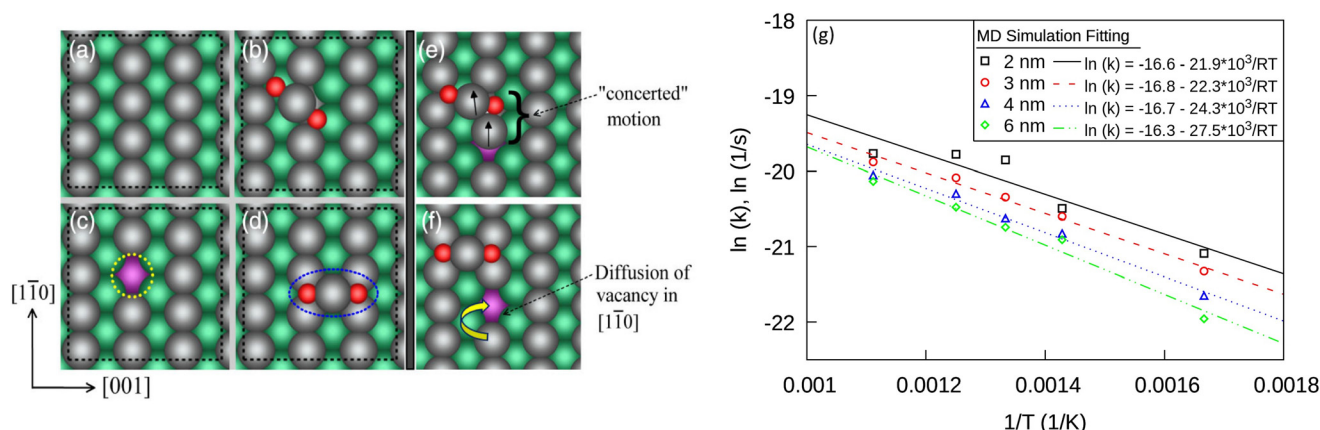

Fig. 2 Ag vacancy formation on a (110) facet: (a) pristine surface, (b) formation of O–Ag–O complex by oxygen dissociation, (c) formation of Ag vacancy, (d) Ag adatom stabilized by oxygen, (e) diffusion of O–Ag–O and Ag atom and (f) diffusion of vacancy. Ag atoms in the first, second and third layer are shown in gray, green, and purple, respectively; O atoms are shown in red (adapted from ref. 160 with permission from the American Physical Society, copyright 2017). (g) Arrhenius plots of the Ag NP oxidation determined by the shrinking core model at 600–900 K (adapted from ref. 161 with permission from the American Chemical Society, copyright 2023).

icity, but also demonstrate enhanced functional performance. For example, iron exhibits remarkable interest for magnetically directed drug delivery and hyperthermia applications, due to its higher magnetic strength compared to the more commonly used iron oxides.[174] However, iron oxidizes easily, is toxic, and tends to aggregate leading to thrombosis.[175] In contrast to pure Fe_{13} clusters that form stable oxides (Fig. 3a) which reduce their magnetic moment, Au coatings prevent Fe oxidation (Fig. 3b), while maintaining the magnetic properties of the core Fe.[174] Similarly, substitutional introduction of Au into the corners and edges of Pt NPs inhibits oxide formation and Pt dissolution in aqueous solution, enhancing its stability.[176] In addition, Au–Co bimetallic NPs with $L1_0$ ordered structure exhibit higher magnetic anisotropy energy compared to core–shell or disordered (alloyed) ones, highlighting potential for magnetic NP hyperthermia applications.[177] Recently, ReaxFF MD simulations[178] revealed that even though

the crystal phase and metallic core are preserved during early stages of sintering of Ni/NiO and Cu/Cu_2O metal/metal oxide core–shell NPs, the iron core in Fe/Fe_2O_3 NPs is fully oxidized due to higher oxygen mobility (Fig. 3c).

The effect of the local surface structure on NP physico-chemical stability has also been demonstrated by DFT and electronic structure calculations of metal oxides, such as CeO_2[179] and TiO_2.[180] Oxygen diffusion leads to disordered but partially stable CeO_2 oxide surfaces, which are further stabilized by water adsorption.[179] Furthermore, water molecules preferentially bond to low coordinated atoms of the TiO_2 surface, enhancing the overall NP stability.[180] Coordination analysis of surface Ti atoms indicated that smaller NPs exhibit more undercoordinated Ti (coordination number <6) and less fully coordinated Ti atoms, enhancing the overall NP affinity to water adsorbates (Fig. 4).
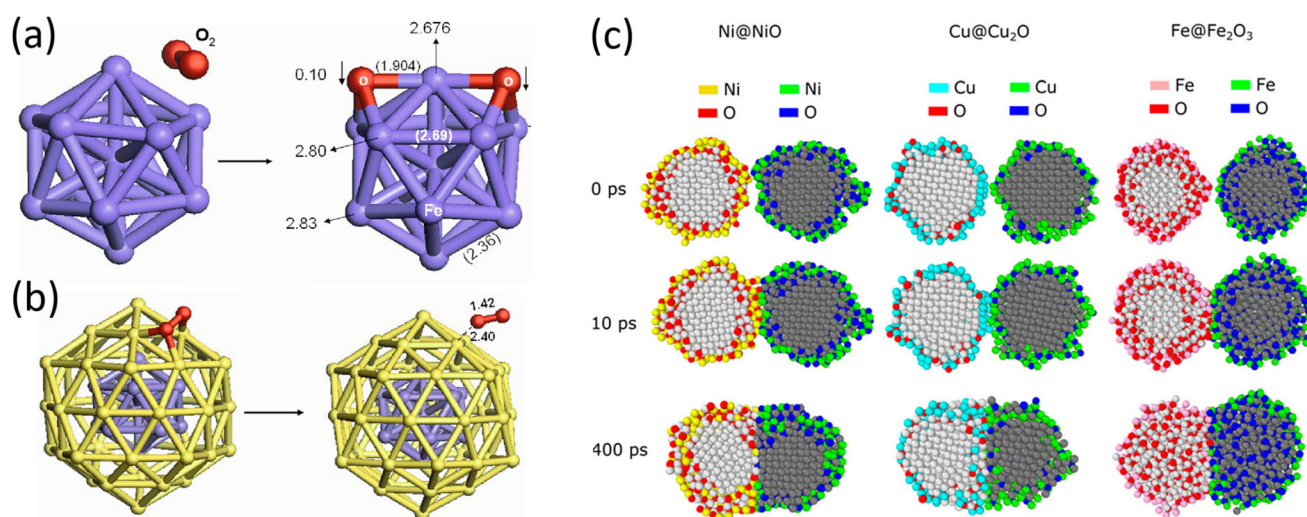

Fig. 3 Initial and optimized geometries for (a) $Fe_{13}–O_2$ and (b) $Fe_{13}@Au_{42}–O_2$.[174] The bond lengths (Å) (in parentheses) and magnetic moments are given for $Fe_{13}–O_2$, while the bond length of O_2 and the distance between $O_2–Au$ are given for $Fe_{13}@Au_{42}–O_2$. Purple: Fe, red: O, and yellow: Au. (c) Cross section snapshots of two coalescing core–shell NPs. Atoms are colored based on their initial position (core, surface, starting NP), with O atoms shown in red (left NP) and blue (right NP, adapted from ref. 178 with permission from the American Chemical Society, copyright 2021).
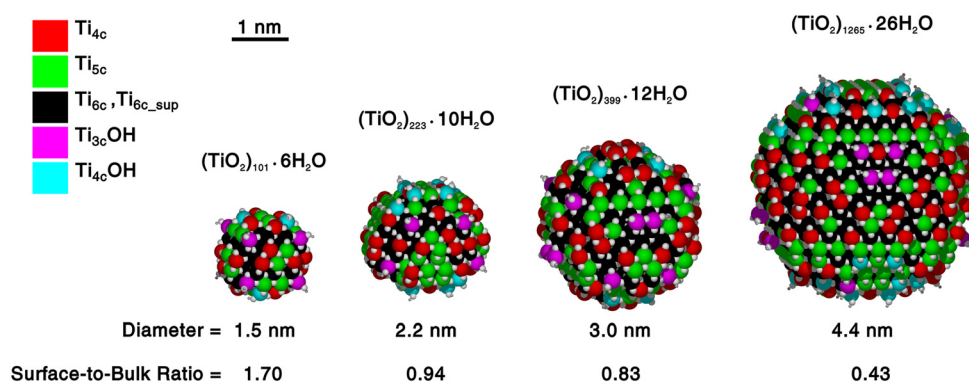

Fig. 4 DFT-optimized geometries of anatase TiO_2 NPs, corresponding to the most stable configurations after annealing at 300 (diameters of 1.5 and 2.2 nm) and 500 K (3 and 4.4 nm). Color code shows different coordination types for surface Ti atoms (adapted from ref. 180 with permission from the American Institute of Physics, copyright 2017).

2.2 Nanoparticle interactions in solutions: surface reactivity, dissolution, and thermal properties

Evaluation of nanoparticle properties in solutions, such as dissolution and surface reactivity, is crucial for biomedical applications due physiological constraints. For example, surface reactivity affects the properties of nanocarriers in drug delivery, while nanoparticle solubility (or dispersibility) affects their compatibility with biological systems. Poor solubility promotes aggregation which, in turn, limits NP interactions with target cells or tissues. However, controlled NP dissolution is often desirable for antibacterial activity.[181]

Reactive MD using COMB3[182] has shown that the degree of Pt NP oxidation affects its dissolution. Pt NPs with low fraction of oxygen adsorbates (<40%) on surface atoms release multiple highly charged Pt ions (Fig. 5a: red ions with q = +0.85e), while evenly sized Pt NPs with high oxygen coverage (>60%) do not dissolve. Water absorbs on Pt(111), (100), (110), (211), and (321) surfaces via the oxygen atom (Fig. 5b),[183] and dissociates more easily on the (110) Pt surface than on (111), underscoring the significance of both the surface facet and coordination in Pt reactivity. The Pt(110) surface is more active than the (321)

facet, similar to Ag surfaces.[184] In anatase TiO$_2$, water dissociation occurs at bridging oxygen sites, forming hydroxyl groups.[185] These sites on the edges and corners on the TiO$_2$ NP facilitate faster water adsorption and desorption cycles compared to flat surfaces. Spontaneous dissociative adsorption of water on both anatase and rutile TiO$_2$ nanosurfaces has also been observed, leading to formation of hydroxyl and hydrogen ions.[186] These computational insights are crucial for understanding water interactions with TiO$_2$ surfaces in physiological media and highlight the potential for surface functionalization to enhance biocompatibility in drug delivery applications. CeO$_2$ NPs, studied by MD simulations and DFT calculations, exhibit increased reactivity at higher Ce^{3+}/Ce^{4+} ratios and oxygen vacancies in CeO$_2$, as highlighted by electrostatic potential maps (Fig. 5c–f).[187] This makes CeO$_2$ NPs susceptible to oxygen release in the presence of water, a property that can be exploited to enhance their effectiveness as nanocarriers in drug delivery.

The physicochemical properties of nanomaterials can also influence the thermal performance of nanofluids in medical applications. Enhanced thermal conductivity can optimize drug release,[188] aid cancer treatment with radiofrequency abla-
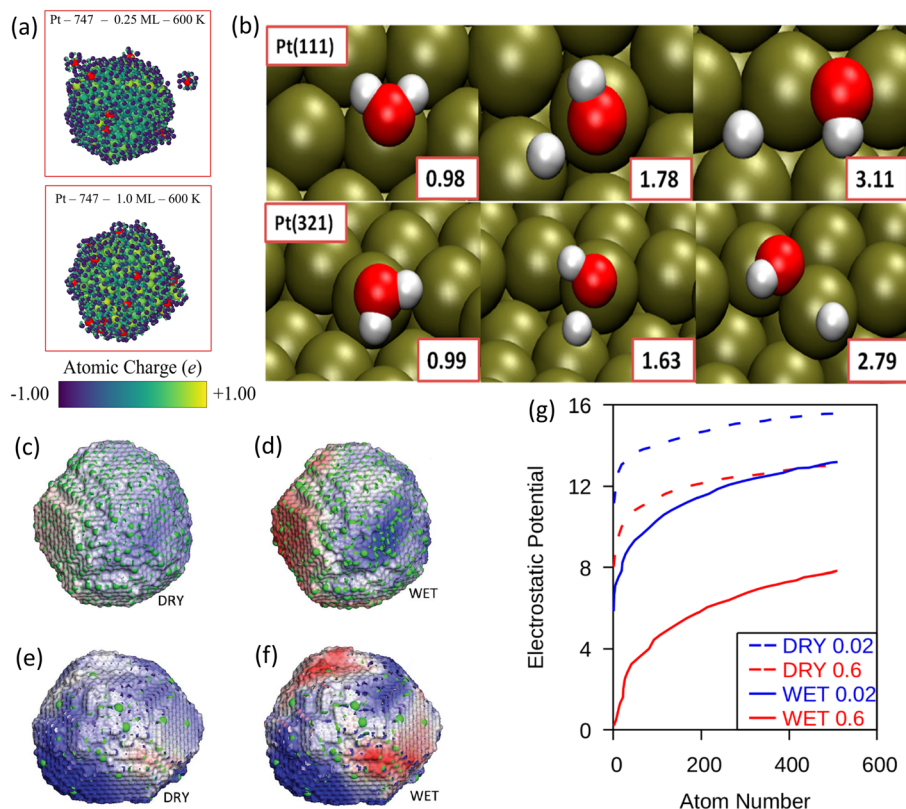

Fig. 5 (a) Dissolution of Pt NPs with different coverage of atomic oxygen monolayer, color-coded based on atomic charge (adapted from ref. 182 with permission from the Royal Society of Chemistry, copyright 2023). Atoms with a charge higher than 0.85e⁻ (red) dissociate from the monolayer at low oxygen coverage but not at higher levels. (b) Optimized geometries for the initial (left panel), transition (middle panel), and final states (right panel) of water dissociation on (111) (top) and (321) Pt facets (bottom), along with the cleaved O−H bond distances in Å (white: H, red: O, green: Pt) (Adapted from ref. 183 with permission from the American Chemical Society, copyright 2014). (c−f) Electrostatic potential maps of (c and e) dry and (d and f) wet CeO$_2$ NPs with Ce^{3+}/Ce^{4+} ratio of (c and d) 0.6 and (e and f) 0.02.[187] Green spheres represent the positions of Ce^{3+} ions. (g) Calculated electrostatic potentials of the CeO$_2$ NPs of Fig. 5 (c−f) (adapted from ref. 187 with permission from the Royal Society of Chemistry, copyright 2013).

tion,[189] and improve flexibility of biological tissues during peristalsis facilitating endoscopy procedures.[190,191] Efficient heat transfer from nanomaterials to surrounding liquids is crucial in diagnostic tools, photothermal therapies, and drug delivery devices.[192,193] The thermophysical properties of nanofluids depend on NP characteristics such as size[194] and morphology.[195] MD simulations have shown an increase in the specific heat capacity of Cu NP-water nanofluids for NP sizes of 1–10 nm,[194] approaching the bulk heat capacity for NPs larger than 4 nm. Addition of Cu and CuO NPs in water-based nanofluids increases the thermal conductivity by forming a heat-conductive channel around the immersed nanoparticles.[196] This is consistent with MD simulations[197] of Pt zig-zag nanochannels containing water and Cu NPs, where NPs demonstrated a preference to accumulate near the nanochannel walls, leading to increased density and thermal conductivity of the nanofluid, accompanied by a decrease in the temperature and molecular velocity of the nanofluid. Similar effects have been observed for CuO[198] and Fe_3O_4 NPs.[199,200]

The chemical environment within aqueous suspensions is also key in dictating the behavior of these engineered nanomaterials by altering their morphology and surface reactivity. The relationship between NP size and its impact on reactivity and toxicity is illustrated by MD simulations of 1–20 nm Ag NPs in water,[201] revealing that smaller particles exhibit higher surface energy, making them less stable. Interestingly, within the 3–10 nm range, hybrid structures with high surface energies were identified, indicating that the reactivity and toxicity of small Ag NPs can change significantly even for slight size variations in current analytical methods. The roughness of such Ag NPs increases with increasing number of atoms, peaking at 8000 atoms before decreasing as the number of Ag atoms grow further, indicating an optimal particle size for NP roughness which affects NP interactions with ligands and biomolecules. Rough surfaces provide more stabilizing contacts compared to smooth surfaces,[202] enhancing binding efficiency and surface reactivity.

2.3 Antibacterial activity

Molecular dynamics and molecular docking simulations have been crucial in understanding the antibacterial activity of Ag NPs and their interactions with bacterial components. Such calculations have identified likely regions that nanosilver interacts most effectively with different bacteria,[203] and have elucidated the mechanism of Ag NPs cytotoxicity stemming from their interactions with proteins involved in apoptosis and oxidative stress generation.[204] Furthermore, coarse-grained MD simulations demonstrated that when Ag nanoclusters (<1 nm) are coated with amphiphilic ligands, they exhibit superior antibacterial effects due to overcoming energy barriers more easily than Ag NPs larger than 2 nm.[205] IR spectra measurements supported by MD simulations[206] indicated enhanced stability of Ag NP-nisin conjugates, due to stronger interactions between the N-terminal residues of nisin peptide and the NP core. In contrast, C-terminal residues are dominated by non-covalent interactions with the anionic membrane that destabi-

lize the NP when it interacts with the cell membrane of bacteria.

Modification of Ag surface with polymers, such as poly(*N*-vinyl-2-pyrrolidone) (PVP) and chitosan, enhances the stability and antibacterial activity of Ag NPs by preventing aggregation. Tang *et al.*[207] explored the adsorption of Ag NPs on activated carbon fibers using chitosan as binding agent, demonstrating excellent antibacterial activity. Fig. 6a–f shows coarse-grained MD simulations of the adsorption of Ag NPs on chitosan-coated carbon fibers, forming small aggregates comprised of 1 to 5 NPs, leading to a decrease in their surface area. These clusters attach to chitosan chains, which transition from stretched to wrapped configurations around the cluster, leading to Ag NP deposition on the carbon, in accord with scanning electronic microscopy images (Fig. 6g and h).[207]

2.4 Nanoparticle-based drug delivery

One of the game-changing applications of nanomaterials lies in targeted drug delivery. The discovery of new drug candidates is a slow and expensive process, taking years to identify a viable candidate.[208] When using NP formulations, multiple variables must be taken into account, such as NP solubility (as discussed in section 2.2), drug loading capacity, release kinetics, functionalization, and interaction with biological targets. Computational approaches can accelerate the discovery of new drug candidates and improve the design of appropriate nanomaterials by predicting their properties and behavior in biological media. For example, McLean and Yarovsky[209] have outlined the physicochemical[210] and biofouling[211,212] properties of functionalized silica, illustrating its potential for biomedical applications. Computational screening of ligand-functionalized surfaces allowed for evaluation and selection of amorphous silica surfaces that resist protein adsorption, critical for developing efficient biomedical devices.[212] Both MD and experiments have revealed that silica NPs can translocate through giant unilamellar vesicles when exposed to high-frequency electromagnetic fields. This was also observed by MD and experiments, highlighting the impact of electromagnetic fields on enhancing membrane permeability, opening new possibilities for precise targeted drug delivery.[210]

CGMD simulations have revealed that nanoparticle targeting of lipid membranes is influenced by various factors. Globular proteins adsorb on NPs in orientations that maximize contact between aminoacids and the NP surface.[213] The permeation of fcc NPs in intestinal membranes varies with NP shape and surface charge. Nonpolar rod-shaped NPs cross the lipid membrane model more easily compared to spherical and disc-shaped ones, while polar NPs were unable to permeate the membrane regardless of their shape.[214] Additionally, CGMD simulations with the MARTINI model[215] have shown that the length and density of ligands in functionalized NPs with hydrophobic cores can tune their location in membranes. Hydrophobic NPs tend to occupy the raft domain of membranes while less hydrophobic NPs occupy the non-raft domain. Larger ligands can also affect the localization by hindering the exposure of NP's hydrophobic core.
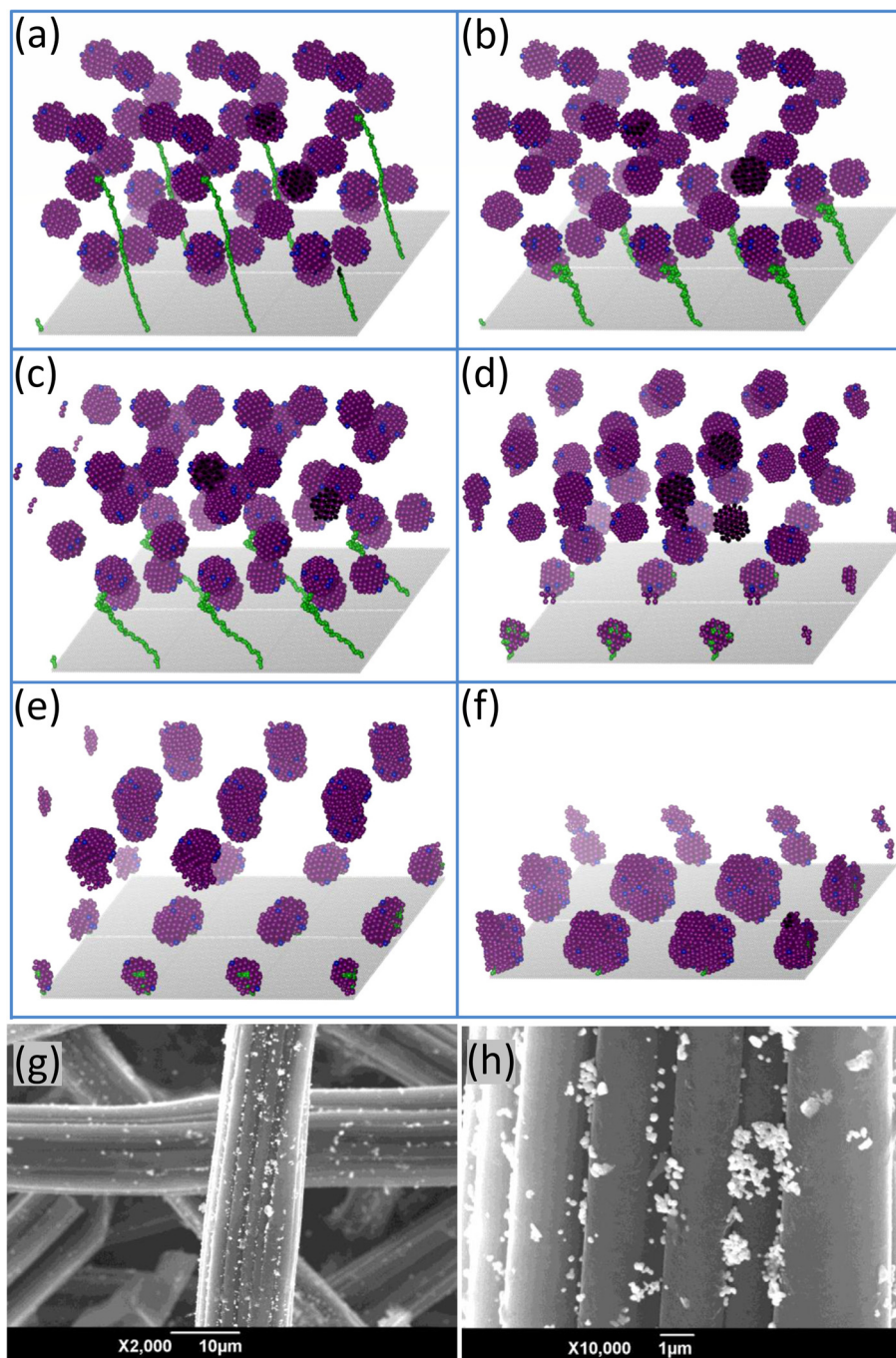
Fig. 6 (a–f) Adsorption of Ag NPs on chitosan-active carbon fibers (purple: non-charged Ag NPs, blue: negatively charged Ag NPs, green: chitosan monomers, silver: carbon surface) and (g and h) scanning microscopy images of Ag NPs supported on carbon (adapted from ref. 207 with permission from Elsevier, copyright 2017).

Biocompatibility and biodistribution are essential in nanocarrier applications. Natural rubber latex has been shown to improve Ag NP biocompatibility, increasing the release of anti-inflammatory molecules, such as metronidazole (MET),[216] with potential in the treatment of bone or tissue infections. Simulations and experiments[217] revealed that MET-Ag NP interactions are favored over rubber-Ag NP ones, as indicated by the local softness in rubber latex (Fig. 7a) and MET mole-

cules (Fig. 7b), corroborated by *in vitro* experiments of MET release.

Surface coatings, such as poly-(ethylene glycol) (PEG), are commonly employed to increase NP stability, improve cellular uptake, reduce the toxicity of nanocarriers, and prevent unwanted interactions with biomolecules. MD, DFT, and simulated annealing Monte Carlo (MC) simulations have illustrated the adsorption of PEG molecules on Ag NPs, identifying
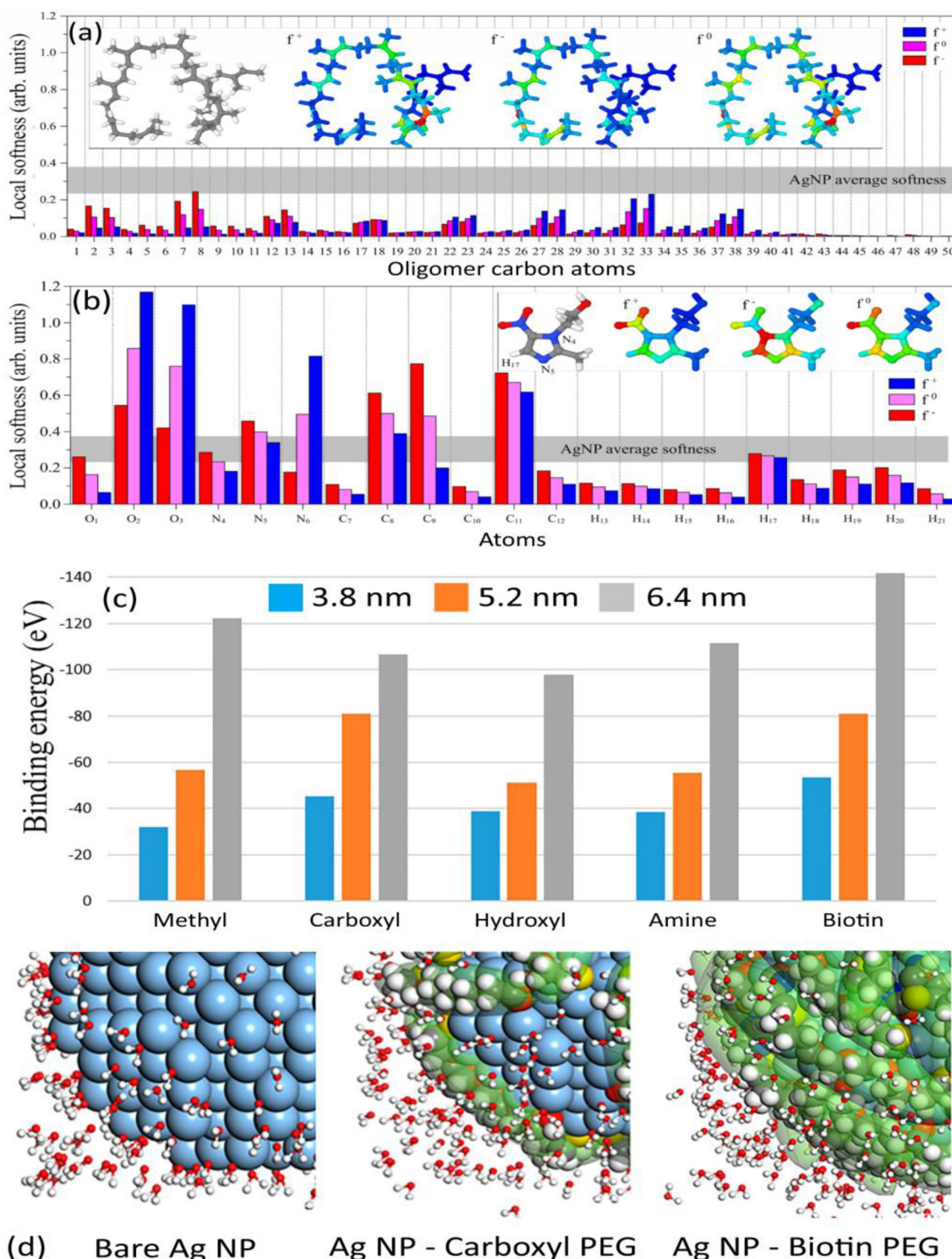
Fig. 7 Local softness as a function of atom type for (a) natural rubber latex and (b) MET molecule for the Ag NP functionalization (adapted from ref. 217 with permission from Springer Nature, copyright 2022). (c) Binding energy as a function of the number of functionalized PEG ligands on Ag NPs.[218] (d) Direction of oxygen in water molecules during interactions with a 6.4 nm Ag NP (blue: Ag, red: O, white: H, and green: carboxyl or biotin functionalized PEG ligands) (adapted from ref. 218 with permission from Taylor and Francis, copyright 2023).

methyl, hydroxyl, carboxyl, amine, and biotin functional groups as reactive centers.[218] Larger Ag NPs exhibited lower binding energies for all functional groups (Fig. 7c), but the car-

boxyl and biotin groups affected the directionality of water molecules (Fig. 7d), resulting in the most stable Ag NP-PEG structures. This potentially leads to water deprotonation and

local pH changes, impacting the cellular media. Similarly, PEG-coated Fe_3O_4 NPs loaded with 5-fluorouracil demonstrated that NP coating and size can tune drug delivery.[219]

Multiscale modeling[220] of PEGylated Au and Ag NPs revealed that increasing the density of PEG coating weakened NP-protein binding, while proteins exhibited preferential coating towards pristine Ag NPs rather than pristine Au. Simulations of immobilized proteins on Au NPs at various rotation angles (Fig. 8a–c) revealed that side chain interactions can guide the design of nanocarriers and nanosensors. Such multiscale approaches have been employed to optimize nanocarrier design targeting tumor cells, by estimating the binding energies between blood plasma or various dietary proteins and Ag NP surfaces.[221] The simulations have shown that biomolecule adsorption is more favorable on the (110) and (111) Ag NP facets rather than (100) ones, with aromatic residues showing strong binding on the (111) facet due to its electron density distribution, whereas linear molecules bind more strongly on the (110) facets (Fig. 9a). Such efficient screening of biomolecule interactions with different NP surfaces can aid in the rational design of nanocarriers. Similar computational approaches[222] have shown that TiO_2 NPs favored hydrophilic interactions over affinity to protein residues, while moderate interactions of Au NPs with gelatin[223]

and pectin,[224] primarily through physisorption, showcased their potential as drug carriers for curcumin, an antioxidant compound.

Super-paramagnetic Fe_3O_4 NPs have emerged as promising drug delivery agents due to their non-toxic nature, magnetic resonant activity, biocompatibility, and cost-effectiveness.[225] Their ability to maintain magnetic properties when complexed with polymers like chitosan enhances their potential in theranostic applications.[226] Chitosan's positive charge density enables strong interaction with negatively charged drug molecules, making it an ideal carrier. MD simulations[227] have revealed strong affinity of chitosan with the Fe_3O_4(111) surface, compared to other facets, with hydrogen and nitrogen from chitosan's amino group showing higher interaction probability with oxygen atoms on the (111) Fe_3O_4 facet. Furthermore, experiments and MD simulations of the adsorption of bovine serum albumin (BSA) protein on Fe_3O_4 NPs revealed the formation of multiple protein monolayers on the NP surface, with BSA protein spreading over the Fe_3O_4 NP surface and eventually relaxing into a compact configuration (Fig. 9b).[228] This strong protein adsorption, confirmed by transmission electron microscopy and UV-vis measurements, suggests BSA-coated Fe_3O_4 NPs as highly resistant drug delivery vehicles.
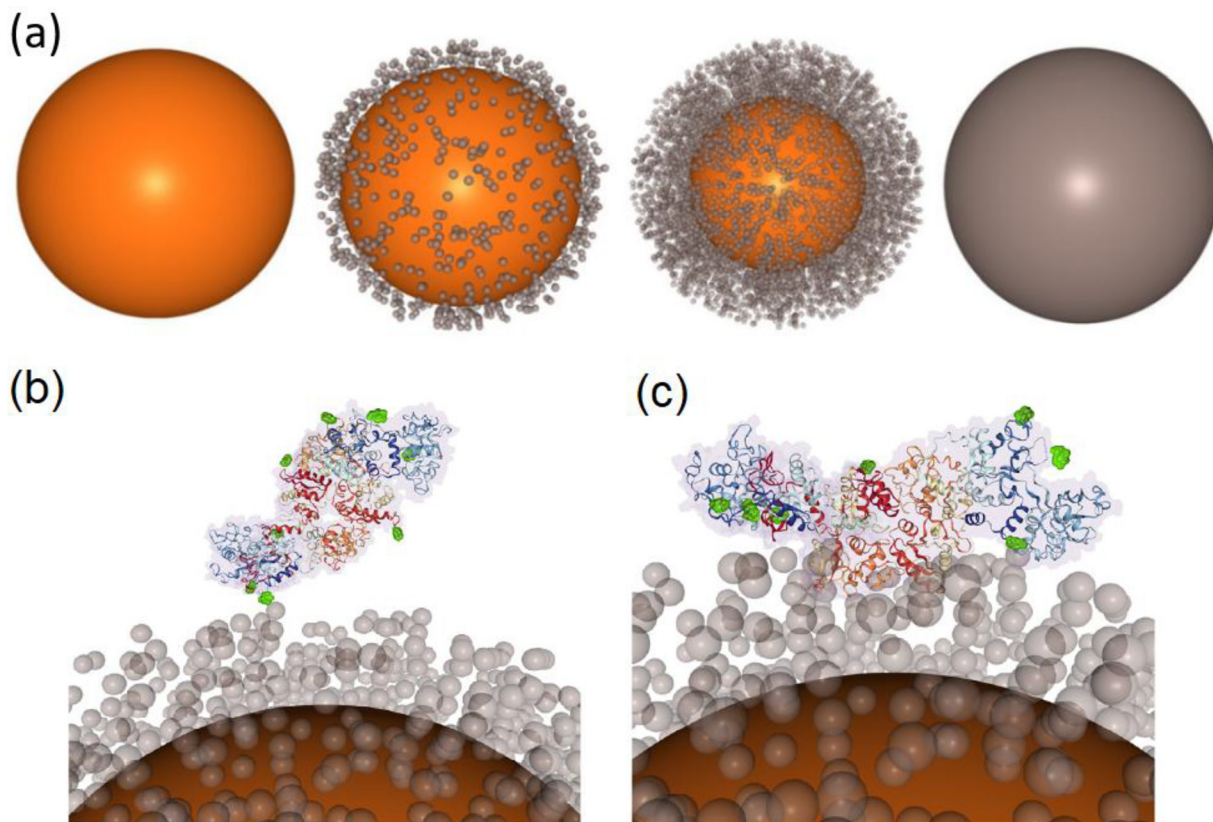

Fig. 8 (a) CG structures of pristine and PEGylated Au NPs. CG structures of docked protein apo-human serum transferrin on PEGylated Au NPs with rotational coordinates (b) φ = 180°, θ = 90° and (c) φ = 200°, θ = 25° (adapted from ref. 220 with permission from the Royal Society of Chemistry, copyright 2023).
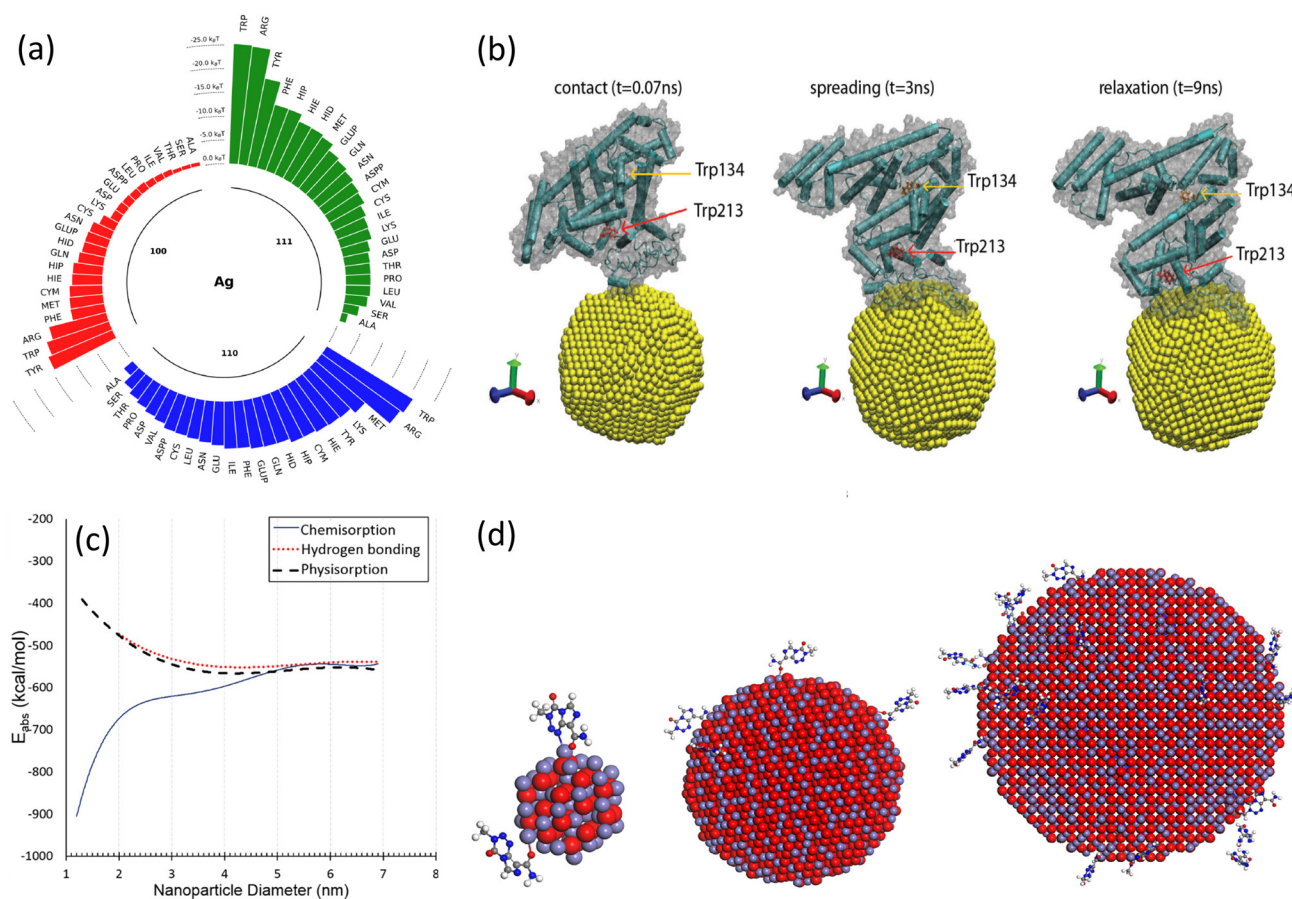
Fig. 9 (a) Adsorption energies (in k_BT) for biomolecules on (100) (red), (110) (blue), and (111) (green) Ag surfaces (adapted from ref. 221 with permission from the American Chemical Society, copyright 2022). (b) Conformational changes of BSA adsorption on a Fe_3O_4 NP (yellow, adapted from ref. 228 with permission from the Royal Society of Chemistry, copyright 2016). (c) Binding energy of TMZ on Fe_3O_4 NPs as a function of NP size.[229] (d) TMZ attains perpendicular orientation on 1.2 (left), 4.2 (center), and 6.5 nm (right) Fe_3O_4 NPs (adapted from ref. 229 with permission from Elsevier, copyright 2019).

Nanoparticles offer targeted delivery solutions for various chemotherapeutic agents, enhancing efficacy while minimizing side effects. For example, functionalized NPs with optimized size and charge can improve brain delivery of Temozolomide (TMZ), which exhibits poor permeability in the brain. DFT/MD studies[229] have shown that Fe_3O_4 NPs smaller than 4 nm enhance TMZ permeability through chemisorption (Fig. 9c) and potential modification of TMZ's charge distribution, while for larger NPs chemisorption, physisorption, or hydrogen binding may occur. Chemisorption can result in modifications in the molecular structure of the drug molecule, whereas physisorption and hydrogen bonding leave the TMZ molecule intact, preserving its physical properties upon its release from the nanocarrier. The Fe_3O_4 NP loading capacity also varies with NP size, favoring a perpendicular TMZ configuration on the NP surface (Fig. 9d). Similarly, Doxorubicin (DOX), another widely used chemotherapeutic agent, which poses challenges due to its cardiotoxic side effects benefits from the encapsulation of TiO_2 nanotubes, that facilitate DOX aggregation within the nanotube as confirmed by DFT/MD simulations,[230] thereby reducing interaction with the cardiac

tissue. Furthermore, Phenindione, an anticoagulant with severe side effects, can be effectively incorporated into galactose-loaded Ag NPs, promoting slow release and slowing down blood coagulation, as demonstrated by DFT calculations of galactose-phenindione interactions.[46] Similar *in silico* studies have been reviewed by Ashwini *et al.*[231]

In antiviral and antibacterial therapies, NP-based approaches can mitigate side effects while enhancing therapeutic efficiency. Morad *et al.*[232] explored the adsorption of COVID-19 therapeutic agents, hydroxychloroquine and chloroquine, on various metallic NPs (Ag, Au, Ag/Au, and Pt NPs) by QM and MD. The hydroxyl group in hydroxychloroquine exhibited the strongest binding on Pt. Increasing Ag NP size from 1.6 to 4.6 nm led to weaker interactions with both drugs. Among metal clusters of 147 atoms and different compositions, affinity followed the trend: Ag NP < AuAg NP < Au NP < Pt NP.

2.5 NP-based computer simulations for neurodegenerative disease treatment

As these advancements in understanding NP behavior in biological systems continue, there is increasing attention towards

specialized medical challenges, such as treatment of neurode-generative diseases. Alzheimer's (AD) and Parkinson's disease (PD) share features including accumulation of proteins in cells (amyloids), abnormal metal ions concentration in cerebral media, and high oxidative stress levels in the brain.[233] Although a handful of drugs approved by the U.S. Food and Drug Administration are available for clinical use, their thera-peutic benefits are short-lasting and unable to halt disease progression.[234] The urgency to develop more effective treat-ments against neurological disorders has led researchers to explore multitarget strategies including nanomaterials. Computational simulations have proven essential in under-standing complex interactions between biomolecules and nanocarriers, helping optimize drug design. However, most

computational research has centered on molecular drug design,[235–237] with less emphasis placed on inorganic NPs, despite their potential in drug distribution.[238] A major chal-lenge in AD and PD drug design is ensuring that drug candi-dates cross the blood–brain barrier (BBB) while designing nanocarriers that avoid undesirable interactions during this BBB crossing.

One of the main hallmarks of AD is the aggregation of unfolded amyloid-beta (Aβ) monomers into fibrils that interact with NPs. Tavanti et al.[239] explored by MD the interaction between Aβ 40 monomers and citrate-capped Au NPs in water. Contact probability analysis between the functionalized Au NP and 1–3 Aβ monomers (Fig. 10a, top), revealed two binding Aβ sites, $^{13}HHQK^{16}$ and $^{24}VGSNKGAI^{31}$, with more binding sites
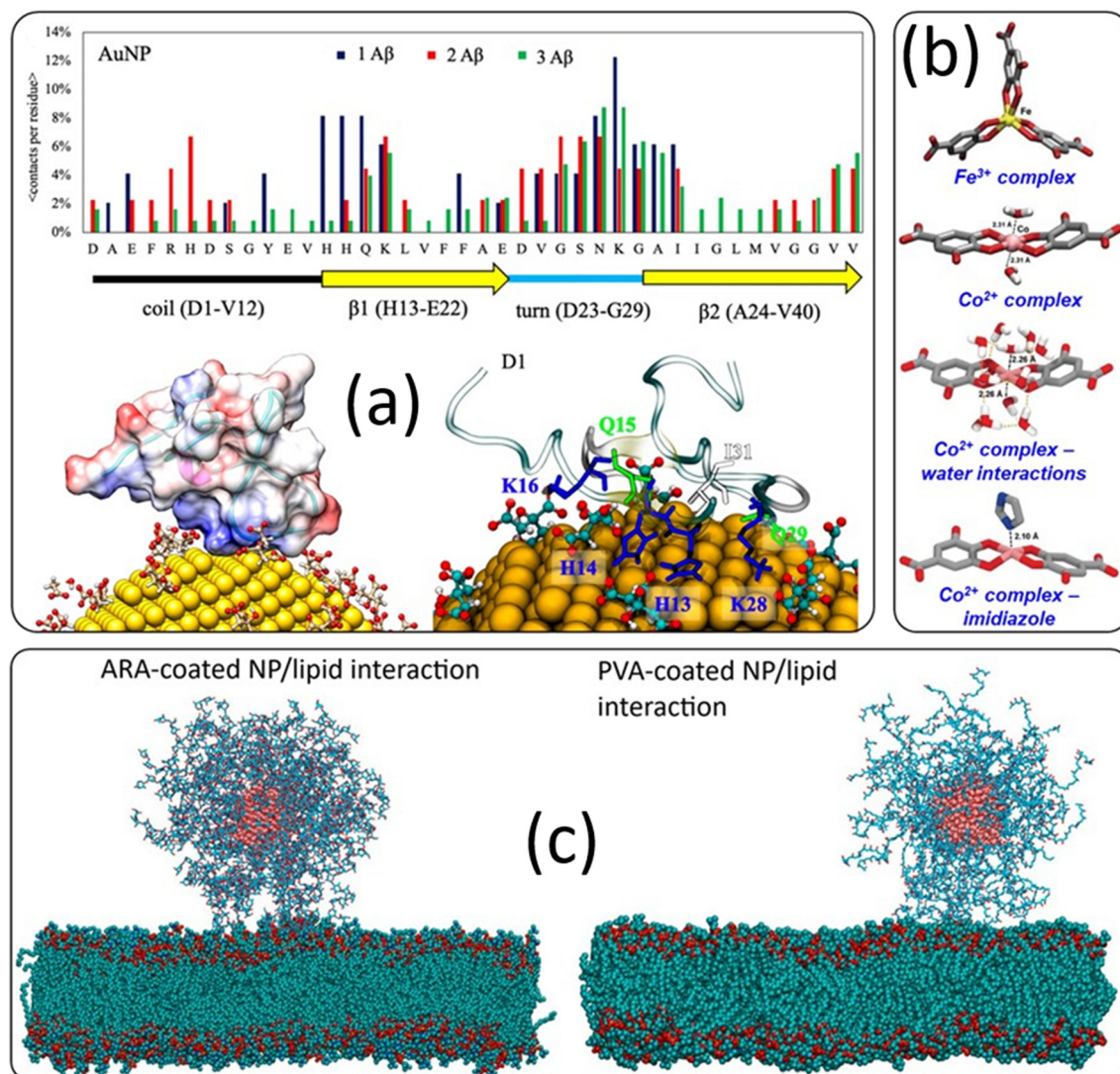

Fig. 10 (a) Contact probability between AuNP and Aβ (1–40) residues for three different amyloid concentrations (top); Au NP-Aβ complex interact-ing with Aβ, showing the surface potential map of Aβ (bottom-left) and amino acid residues involved during Aβ attachment to the Au NP surface (bottom-right). Negatively charged residues are shown in blue (adapted from ref. 239 with permission from MDPI, copyright 2021). (b) Structures of Fe (yellow) and Co (pink) complexes with tannic acid in the presence of water molecules and imidazole ring of histidine (adapted from ref. 241 with permission from the Royal Society of Chemistry, copyright 2019). (c) Interaction between lipid layer model and Fe_3O_4 NP coating with ARA and PVA (adapted from ref. 243 with permission from Elsevier, copyright 2020).

observed as the number of Aβ monomers increased, including a C-terminal contact site. Positively charged Aβ regions (K28, H13, H14, and K16) interact with negatively charged citrate ligands (Fig. 10a, bottom left), while other residues (Q15, Q29, and I31) bind to Au atoms *via* van der Waals forces (Fig. 10a, bottom right). These interactions disrupted Aβ aggregation, highlighting the potential role of Au NPs in altering AD-related protein aggregation, with similar results seen in MD studies relevant to PD.[240] Zhang et al.[241] synthetized Au NPs coated with metal-phenolic networks, with inhibitory activity towards amyloid formation. Polyphenolic networks between tannic acid and different metal ions (Al^{3+}, Fe^{3+}, Co^{2+}, Ni^{2+}, Cu^{2+} and Zn^{2+}) were explored, with cobalt–tannic acid complexes exhibiting the highest inhibitory activity. MD simulations revealed Co complexes with uncoordinated axial positions allowing them to interact with water molecules and amyloid amino acids (Fig. 10b, top). In contrast, iron complexes formed stable octahedral structures, reducing solvent exposure. QM calculations showed that while water interactions with Co centers were unfavorable, histidine and methionine interact strongly with Co (Fig. 10b, bottom), potentially reducing oxidative stress and preventing Aβ aggregation commonly associated with AD.

To overcome BBB permeability restrictions, non-invasive techniques using magnetic fields have been investigated. Magnetic Fe_3O_4 NPs have emerged as effective contrast agents for magnetic resonance imaging (MRI) for AD or epilepsy diagnosis due to aggregation of these NPs in the brain by the high magnetic activity of the neural network in this zone.[242,243] Lazaratos et al.[243] performed MD simulations and experiments to examine the interactions between lipid bilayers and magnetic Fe_3O_4 NPs coated with polyvinyl alcohol (PVA) and polyarabic acid (ARA) (Fig. 10c). Stronger interactions and shorter Fe_3O_4 NP-bilayer distances were observed for the PVA-coated NP compared to ARA-coated ones. The potential of Au-coated Fe_3O_4 NPs to cross the BBB has also been explored by MD under magnetic fields.[244] The Au/Fe_3O_4 nanocomposites could temporarily open gaps in the membrane, allowing passage and reversible deformation. By adjusting the magnetic field strength and pattern, the BBB crossing time could be precisely controlled, offering significant potential for NP-based treatments targeting the brain.

Parkinson's disease is characterized by dopamine deficiency, leading to loss of coordination and impaired movement. Simulations of Fe_3O_4 NPs for dopamine replacement therapy[245] revealed that as the number of dopamine molecules on uncoated Fe_3O_4 NPs increases, their binding energy increases, though the rate of energy change slows down as more molecules are added. Larger PEG-coated Fe_3O_4 NPs exhibited even higher binding energies with dopamine compared to uncoated NPs, due to the hydrodynamic size increase in the presence of PEG, without sacrificing stability. Furthermore, albumin-coated Fe_3O_4 NPs enhance BBB permeability. Increasing the dopamine-to-albumin ratio at constant PEG led to higher binding energies, indicating stronger ligand-Fe_3O_4 NP interactions. However, increasing PEG for a given amount of dopamine reduced NP stability. These findings suggest that adjusting the ratios of NP coating, dopamine, and albumin offers a potential strategy to optimize NP size and stability for PD treatment. CeO_2 NPs also show potential to inhibit α-syn amyloid aggregate formation, critical in neurodegenerative diseases.[115] Molecular docking and MD simulations revealed strong interactions between CeO_2 NPs and α-syn fibrils. These interactions induced conformational changes in amyloid structure when in proximity to CeO_2 NPs, such as large spacing among neighboring protein chains, leading to partial disaggregation of α-syn, consistent with spectroscopy measurements.[115]

2.6 Other biomedical applications

The physicochemical properties of NPs change upon interaction with biofluids, as proteins adsorb to form a protein corona that affects the NP's biological response. Computational simulations are instrumental in predicting how these interactions affect NP stability, bioactivity, and the formation of the protein corona. For example, multiscale simulations have been employed to examine the formation of a protein corona on 3.2 and 10 nm Ag NPs using the antimicrobial peptide ovispirin-1.[246] Hydrophilic interactions between the NP surface and certain peptide residues were key to the initial adsorption, with water solvation also contributing to the protein anchoring. An adsorption–desorption–readsorption cycle was observed for a 3.2 nm Ag NP, indicating an unstable attachment, while the larger 10 nm Ag NP showed more stable peptide anchoring due to its larger surface area, allowing peptide diffusion and stronger adsorption (Fig. 11a).

Power et al.[247] developed a coarse-grain multiscale model to rank the adsorption affinity of proteins on Au NPs accounting for preferred orientations and the influence of NP size and shape. Rouse and Lobaskin[248] developed a hard-sphere model to mimic protein corona formation on spherical and cylindrical NPs, finding that NP size and geometry affect protein packing and corona composition. Kinetic MC simulations confirmed these results, predicting different protein coverages depending on NP size and shape. Specific surface interactions with some adsorbates can give rise to more complex phenomena, such as enhanced Raman effect. For example, the interaction of PVA with Ag NPs, investigated by DFT,[249] revealed that the hydroxyl oxygen atoms of PVA attach to a 55-atom Ag cluster, without significantly altering the NP surface. Negative binding energies indicated a thermodynamically favorable interaction between the Ag NP surface and PVA, consistent with surface-enhanced Raman scattering experiments.

Even though the biocompatibility of Au NPs makes them suitable for theranostics, their aggregation in physiological media must be prevented to preserve cellular uptake and low toxicity.[250,251] Canepa et al.[252] explored this issue by CGMD simulations of ligand-functionalized 2–4 nm Au NPs interacting with a bilayer that mimics neuronal plasma membrane in physiological salt solution. Fig. 11b shows the spontaneous adsorption of a single functionalized Au NP onto the lipid, altering lipid–liquid phase separation. Larger Au NPs (4 nm) promote the formation of stable aggregates (Fig. 11b) by indu-
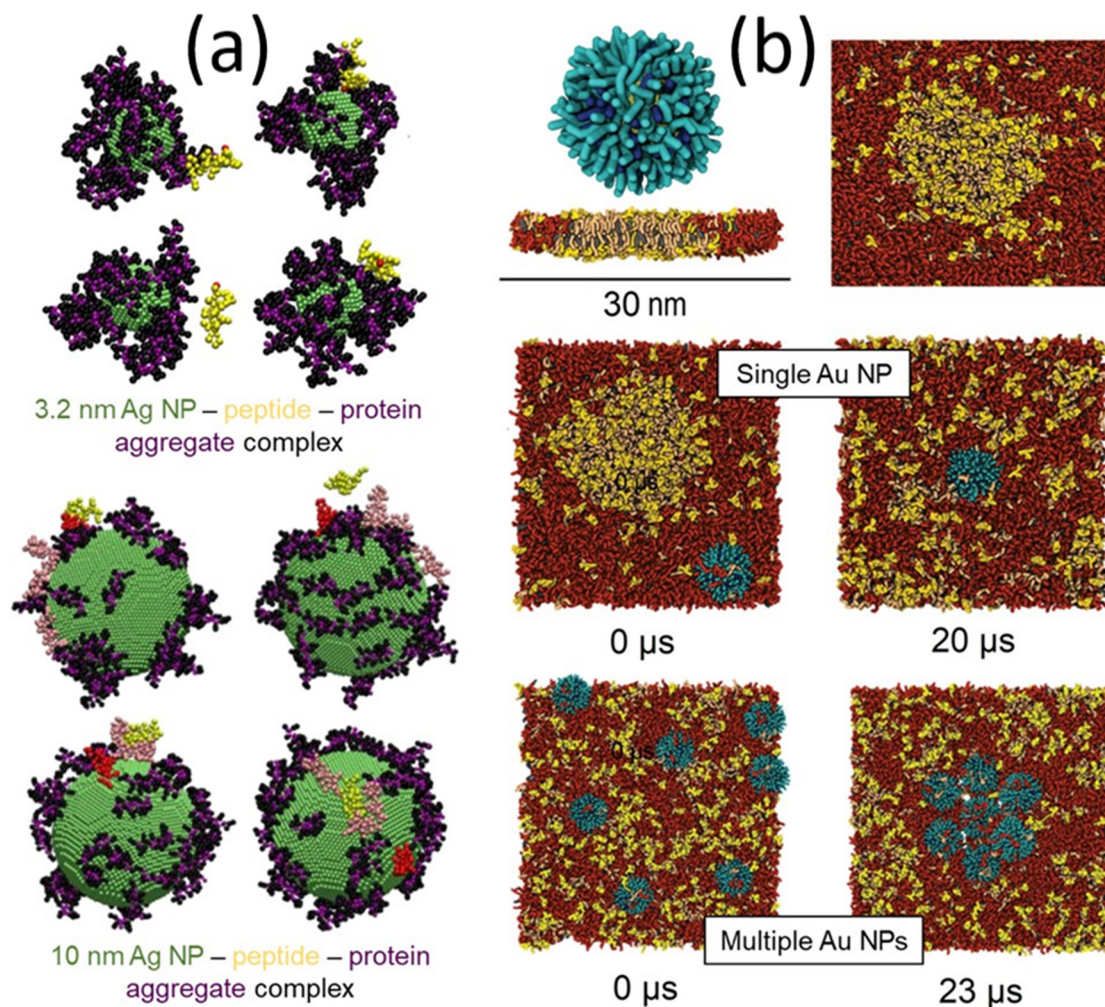
Fig. 11 (a) The adsorption−desorption−readsorption cycle for a 3.2 (top) and a 10 nm (bottom) Ag NP (adapted from ref. 246 with permission from the American Chemical Society, copyright 2022). (b) Coarse-grained representations of NP and lipid bilayer model (top and side views), where hydrophilic ligands are shown in cyan, hydrophobic ligands in blue, glycosphingolipids (gangliosides) in yellow, 1,2-dilinoleoyl-*sn-glycero*-3-phosphocholine in brown, sphingomyelin in pink and cholesterol in gray. The lipid−liquid phase separation when a single 4 nm Au NP is embedded in the bilayer is compared oncean aggregate is formed by clustering of multiple Au NPs (adapted from ref. 252 with permission from the Royal Society of Chemistry, copyright 2020).

cing perturbations in the lipid bilayer, while smaller ones (2 nm) form transient dimers. These results are consistent with CGMD simulations of fullerene aggregation in lipid membranes, showing that increasing fullerene size promotes aggregation.[253] CGMD simulations[254] of functionalized 4 nm Au NPs showed that short-range charge−charge interactions (ion bridging), lipid depletion, and membrane curvature drive aggregation of adsorbed NPs on membranes, confirmed by cryo-electron microscopy experiments. Recently, Ahmed *et al.*[255] studied the assembly of 5–50 nm Au NPs with bacteriophages by the united atom approach,[247] revealing that these composite nanostructures can minimize the formation of biomolecular corona, maintaining the targeting ability in the biological fluids, which is desirable in sensing applications.

The nonmagnetic nature of graphene has drawn interest in biomedical imaging, as the microstrain effects may induced by

NPs may confer magnetic properties on graphene-based nanostructures. Idisi *et al.*[256] explored this effect on the magnetic properties of graphene oxide nanosheets doped with Fe−O from Fe_3O_4 NPs *via* spin polarizable DFT calculations. The negative formation energies obtained for different Fe−O dopant configurations incorporated in the graphene nanosheet proved the stability of these structures, with significant magnetization enhancement when multiple Fe−O sites are present. Spin density distribution and density of states analysis suggested charge transfer leading to interaction among C, Fe, and O atoms. This charge transfer, along with the NP size, likely explains the origin of the enhanced magnetization observed in experiments. Thomas *et al.*[257] explored the structure of resilin-like peptides on graphene by experiments and MD simulations. Such materials exhibit enhanced elastomeric properties and can create artificial muscles or can be used in

Table 2 Summary of simulation studies of NP-macromolecule interactions relevant for biomedical applications. The computational models are described in terms of the force fields for MD and CGMD, and the basis sets and pseudopotentials in DFT

NP	NP characteristics	Computational model	Biomedical relevance	Ref.
Ag	Ag NPs (<3 nm), coated with adamantanethiolates	CGMD: MARTINI FF and Morse potential for water	Interaction between Ag NPs and multidrug-resistant bacteria membranes	205
	10 nm Ag NP	MD: GROMOS96 FF	Efficiency of the antimicrobial peptide nisin upon assembly at Ag NP surface	206
	Ag NPs, chitosan chains coating	CGMD: LJ-Coulombic potentials, implicit solvent model	Mechanism of Ag NP loading on chitosan chains for fabrication of antibacterial materials	207
	PVP 4.5 nm Ag NP	MD: G53a6 FF with DFT and LJ potential	Polymer-capped NPs with tunable properties	263
	2 nm Ag NP functionalized with MET	MD: AMBER FF, DFT: PBE/6-31G (d,p)	MET and Ag NPs supported on biocompatible rubber latex for drug delivery applications	217
	PEG-coated 1–3.2 nm Ag NPs	MD: consistent-valence FF, DFT: PW91, MC	NP size and PEG functionalization effect in Ag NP stability to supress NP aggregation	218
	Ag surfaces, 29.2 and 43 nm Ag NPs	CGMD: INTERFACE and CHARMM36 FFs, UA potential	Evaluation of hydrophobicity and lipophilicity of Ag NPs to predict their toxicity as nanocarriers	221
	3.2 and 10 nm Ag NPs	CGMD: Martini and CHARMM36 FFs	Size and hydrophilicity effects of Ag NPs on peptide corona formation	246
	PVA coated Ag nanocluster (<1 nm)	DFT: PW91	PVA binding on Ag NP surfaces for nanofiber fabrication	249
	2–10 nm thiolate-coated Ag NPs	MD: ReaxFF	Analysis of thiolates adsorption on Ag NPs (111) surfaces for tuned antibacterial properties	264
	25×25 Å^2 (111) Ag slabs surrounded by water and ligands	MD: AgP-CHARMM and CHARMM36m FFs, TIP3P model	Thermodynamics of the adsorption of different capping agents used for surface stabilization of Ag NPs	265
Cu	DNA and small Cu NPs (<1 nm) composites	DFT: B3LYP-PM6, MD: parmbsc1 FF	Size effect of Cu NPs in DNA binding and structure for their use as anti-fungal agents	266
Au	Bare 4 nm Au NPs	CGMD: MARTINI FF	Adhesion of Au NPs on mixed zwitterionic/anionic lipid membranes relevant in biomedical applications	124
	2 nm Au NPs functionalized with thiol ligands	CGMD: MARTINI FF	Adsorption of Au NPs on mixed lipid bilayers to understand their fate in biological fluids	267
	2 nm alkylamines functionalized Au NPs	MC/MD: CHARMM36m FF, CGMD: POL/BMW-MARTINI FF	Interaction between Au NPs and lipid bilayer membranes	268
	2 nm Au NPs functionalized with PEGylated ligands	MD: OPLS-AA FF, LJ and RB potentials	Solvation of PEGylated Au NPs in water which could inhibit corona protein formation	269
	10 atoms cluster to mimic Au NP surfaces	DFT: B3LYP/LanL2DZ pseudopotential	Determination of optimal NP size for high curcumin drug delivery yield	223
	10 atom cluster bonded to pectin chains	DFT: B3LYP/LanL2DZ pseudopotential	Electronic structure and adsorption study between Au NPs and pectin biopolymer to unveil drug delivery activity of coated Au NPs	224
	4 nm citrate-capped Au NPs with Aβ amyloids attached	MD: GROMOS 54a7 FF	Folding mechanism of Aβ amyloids on Au NPs surfaces to understand formation of toxic plaques in AD	239
	12 nm citrate-capped Au NPs bonded with α-syn protein	MD: CHARMM FF	Binding of α-synuclein with coated Au NPs associated with Parkinson's disease treatments	240
	Coated Au NPs (<50 nm) in water	DFT: B3LYP/6-311G, MD: COMPASS FF	Mechanistic insights of the inhibition of Aβ (1–40) amyloids with cobalt–tannic coated Au NPs	241
	2–4 nm coated Au NPs in multidomain bilayer model	CGMD: MARTINI FF	Effect of amphiphilic and negatively charged Au NPs on neuronal plasma membrane for sensing applications	252
	31.5×31.5 nm^2 surface for Au nanorod with placed DNA receptors	CGMD: oxDNA2 model	Effect of DNA receptor density on DNA-modified Au nanorods for bioimaging and drug delivery purposes	270
	Au(100) nanosurfaces	DFT: B3LYP/6-31G, MD: CHARMM FF, TIP3P model	Binding affinities of capping molecules for Au nanorods growth with multiple biomedical applications	271
	Au(111) nanosurfaces	MD: CHARMM22 FF, TIP3P model	Transition of peptide structure on Au NP by variation of aminoacid fragment affects optical properties	272
TiO$_2$	DOX solution confined inside 2.5 nm TiO$_2$ nanotubes walls	DFT: B3LYP/6-311+G, MD: OPLS-AA and SPc FFs	TiO$_2$ nanotubes as controllable drug-delivery systems of anticancer DOX compound	230
	2.2 nm TiO$_2$ and 50 methoxy-PEG polymer chains	DFT: B3LYP, MD: MA and CHARMM36 FFs, CGMD: MARTINI 2 FF	Cell permeation efficiency estimation of TiO$_2$ coated with PEG-based chains	261
	Polymorphs TiO$_2$ slabs	MD: CHARMM36, LJ potential, TIP3P model	Adhesion of Arg-Gly-Asp on TiO$_2$ surfaces for osseointegration applications	273
	2.2 nm anatase TiO$_2$ NP with DOX and hydrophobic ligands	MD: GAFF2 and modified MA FFs, TIP3P model	pH-triggered release of DOX from functionalized TiO$_2$ NPs to assess drug loading capacity	274
	PEGylated 2.2 nm anatase TiO$_2$ NP with folic acid molecules	MD: CHARMM36 and CGenFF	Protonation state and folic acid density effect on the interaction of TiO$_2$ NP-based nanodevices with folate receptors from tumor cells	275
	TiO$_2$ nanosurfaces, 4 nm Anatase NP	CGMD: Slipids FF, TIP3P model	Adsorption of lipids near TiO$_2$ NPs and nanosurfaces relevant to assess their toxicity	276

Table 2 *(Contd.)*

NP	NP characteristics	Computational model	Biomedical relevance	Ref.
Fe_3O_4	PEGylated and bare 1–7 nm Fe_3O_4 NPs	DFT: PW91, MC/MD: pcff and COMPASS FFs	Coating (PEGylation) and size effect on the drug delivery efficiency of Fe_3O_4 NPs	219
	Slab models of Fe_3O_4	MD: COMPASS FF	Adsorption of chitosan chains on Fe_3O_4 crystallographic planes	227
	6 nm Fe_3O_4 NP with BSA proteins attached	MD: CHARMM27 FF, implicit model GBIS	BSA protein adsorption mechanism for super-paramagnetic nanocarrier design	228
	1–7 nm Fe_3O_4 NPs with TMZ	DFT: PW91, MC/MD: pcff and COMPASS FFs	Effect of water and NPs size in the bonding between Fe_3O_4 surface and anti-cancer TMZ compound	229
	2 nm Fe_3O_4 NP coated with 2 Å thick Au shell	MD: CHARMM27 FF, TIP3P model	Application of a magnetic field for the crossing of core/shell Fe_3O_4/Au NP through BBB	244
	3 nm Fe_3O_4 NPs with ARA and PVA in water	MD: CHARMM36 FF, TIP3P water model	Assessment of interactions Fe_3O_4 NPs with model cell membranes for theranostic purposes	243
	1–7 nm Fe_3O_4 NPs functionalized with dopamine compounds	MC/MD: pcff and COMPASS FFs	Bonding of PEGylated dopamine with albumin molecules on Fe_3O_4 NPs to enhance BBB permeation	245
	Graphene oxide nanosheets doped with Fe_3O_4 NPs	DFT: PBE/Vanderbilt pseudopotentials	Fe_3O_4 NPs doping in graphene oxide nanosheets to enhance magnetic properties for theranostic applications	256
CeO_2	2–3 nm CeO_2 NPs and α-syn mono-mers/fibrils	MD: universal FF	Aggregation study between CeO_2 NPs and α-syn amy-loids associated with neurodegenerative diseases	115
Other	35.7 and 52.7 nm PEG-coated Au/Ag NPs	CGMD: UA potential	Protein binding on the surface of PEG-coated NPs for nanocarriers and biosensors design	220
	5–200 nm Au/TiO_2 NPs	CGMD: UA potential	Development of a model for fast estimation of protein affinities on NPs surfaces	222
	Clusters, (111) slabs for Ag/Au/Pt, 1.6–4.6 nm Ag NPs	DFT: PBE-D3/TZP, MD: Gromos53a6, SPC FFs	Adsorption of hydroxychloroquine on Ag, Au and Pt NPs for antiviral properties against COVID-19	232

wound healing. The binding affinities of various peptides indicated the formation of a dimer in solution that inhibits their attachment to graphene. Considering an additional binding domain, however, all peptides significantly increase their binding, which could guide the design of elastomeric nanomaterials

The superior photocatalytic activity of TiO_2 NPs can be exploited in cancer therapy and diagnostics[95] but their broader application is hindered by potential toxicological manifestations observed in mice rats or other animal models.[258,259] TiO_2 functionalization with PEG chains improves their biocompatibility avoiding premature elimination from the blood circulation by adsorption with serum proteins or by phagocytic uptake, enhancing NP efficacy in reaching tumor sites.[260] Atomistic and coarse-grained MD simulations showed that PEGylated TiO_2 NPs are less thermodynamically stable in lipid bilayers compared to polyethylene (PE)- or PE-PEG-coated NPs, which spontaneously migrate to the membrane, regardless of the chemical nature of the terminal group in PE-PEG chains.[261]

Peroxidases play a pivotal role in detoxification by catalyzing the reduction of hydrogen peroxide. While widely used in biosensors, these enzymes are expensive and sensitive to environmental conditions. As an alternative, metallic oxide nanomaterials, particularly iron oxide, offer similar catalytic activity, higher stability and large surface area at a lower cost. Shen *et al.*[262] evaluated the peroxide-like activity for a set of 15 iron-oxide slabs with different facet orientations and Fe vacancies by DFT, revealing dissociation of the chemisorbed H_2O_2 into hydroxyl groups. This led to a predictive chemical

descriptor for peroxidase-mimicking nanomaterials, in accordance with experimental data, proving the ability of computer simulation to aid the rational design of nanomaterials. Table 2 provides a summary of simulation studies of NP-macromolecule interactions relevant for biomedical applications, classified by nanomaterial type.

3 Multiphysics mesoscale modeling

The atomistic and coarse-grained simulations covered in section 2, usually model small systems of spherical NPs. However, fractal-like aggregates, typically in the range of tens to hundreds of nanometers, are often encountered in complex biomedical environments, where they interact with each other and with external fields, or are dispersed in solutions. In such scenarios, multiphysics mesoscale models can bridge experimental parameters and NP characteristics, helping to uncover structure–property relationships and optimize NP design. Various modeling approaches are available to address different aspects of NP behavior and performance. Discrete element method, Brownian dynamics, and continuum particle dynamics are commonly used to model NP dynamics during their synthesis,[277] focusing on particle movement, interparticle forces, and their collective behavior over time. These simulations offer insights into NP agglomeration[278,279] and transport behavior of irregularly shaped aggregates.[280] Applications of these techniques span from nanotoxicology[281,282] and eco-toxicology[283] to engineered nanofluid stability.[284]

Brownian dynamics, for example, have been used to predict the settling velocity of fractal-like SiO_2 aggregates (Fig. 12a and b) suggesting a linear relationship with the ratio of the agglomerate mass to hydrodynamic diameter (Fig. 12c).[280] However, the assumption of monodisperse primary particles often made in settling rate calculations[285,286] underestimates their settling velocity, as particle polydispersity and agglomerate morphology can significantly influence NP transport. For instance, in agglomerates with a polydispersity of 1.5 and a mass mobility exponent of 2.2 (*i.e.*, open fractal-like aggregates), assuming monodisperse particles can lead to a 33% underestimation of settling velocity. This can potentially result in underestimating NP dose assessment in nanotoxicology studies or overestimating nanofluid stability. Ma *et al.*[287] explored the size-dependent dissolution of Ag NPs, by mass transport rate equations assuming first-order kinetics of Ag ion release. A faster volumetric reduction percentage was observed for octahedral Ag NPs compared to rods and cubes (Fig. 12d–f), corresponding to higher ion release rate, owing to the varying fraction of reactive edges and corners on NPs surface which are more prone to dissolution, as revealed by *ab initio*[287] and reactive MD.[162] Higher NaCl concentrations accelerate Ag^+ dissolution (Fig. 12d) by the increase of the

mass transfer rate of Cl^-. Similar first-order kinetics analysis was used to evaluate leaching from alloyed Ag–Au NPs.[288] Considering a shrinking-particle model, the continuous decrease in NP diameter was predicted along with enrichment in Au during the initial stages of dissolution. These leaching rate results combined with Mie theory simulations of scattering spectra were able to reproduce experimental leaching profiles.

Furthermore, multiphysics models are essential for understanding NP performance in external fields, such as electric[289] or magnetic fields.[290,291] Monte Carlo (MC), 3D full-wave computational models, or discrete dipole approximation techniques are commonly employed to evaluate the optical performance of plasmonic NPs, sought after for non-invasive photothermal therapies and thermally modulated drug delivery, while recent advancements in the simulation of light scattering[292] have increasingly focused on accelerating calculations to larger particles or more complex NP systems, such as NPs near planar surfaces.[293] For example, finite-difference time-domain and finite element method (FEM) have been used to predict the absorption spectra and charge distribution of Fe@Au core–shell nanostars under near-infrared (NIR) irradiation (Fig. 13a).[294] NIR irradiation along the longitudinal
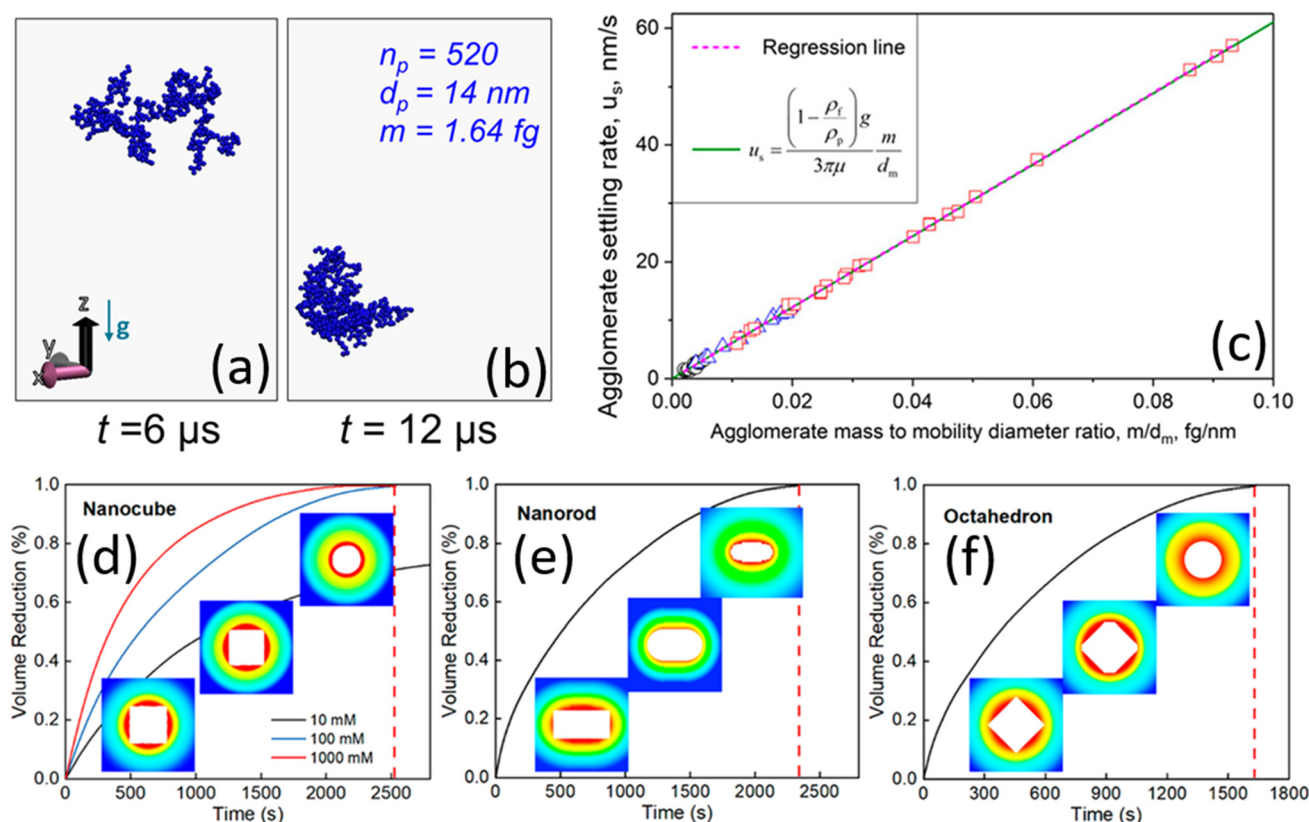

Fig. 12 (a–c) Brownian dynamics settling simulation of a fractal-like SiO_2 agglomerate at (a) 6 and (b) 12 μs. The agglomerate settling rate, μs, scales linearly with the agglomerate mass to mobility diameter ratio, m/d_m (c) (adapted from ref. 280 with permission from the American Institute of Physics, copyright 2018). (d–f) COMSOL multiphysics simulations of the volumetric reduction of Ag (d) nanocube, (e) nanorod, and (f) octahedron during dissolution (adapted from ref. 287 with permission from the American Chemical Society, copyright 2023).
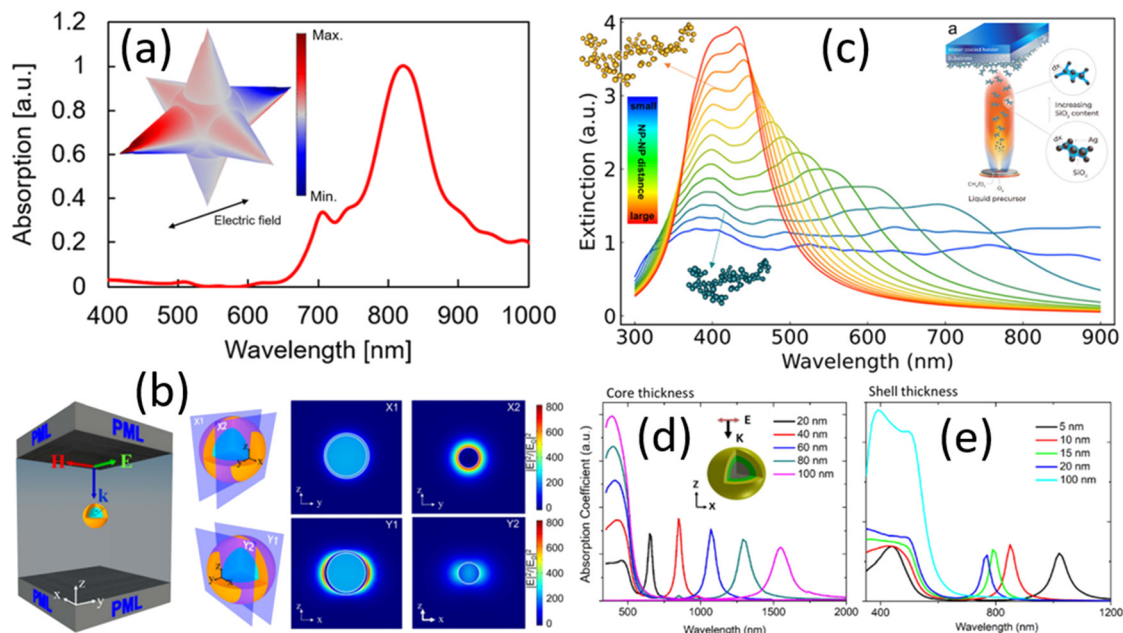
Fig. 13 (a) Simulated absorption spectrum of magnetic core–Au shell nanostar under NIR irradiation and charge distribution at the resonance wavelength (inset, adapted from ref. 294 with permission from Nature Portfolio, copyright 2020). (b) Local field enhancement of the SiO$_2$@Au core–shell structure at the localized surface plasmon resonance wavelength of 800 nm (adapted from ref. 295 with permission from Nature Portfolio, copyright 2016). (c) Simulated extinction spectra of fractal-like Ag agglomerates with different interparticle NP–NP distance.[296] The inset shows nanoaggregates with large (yellow, top-left inset) and short (green, bottom-left inset) interparticle distances and a schematic of flame aerosol deposition experiments of as-prepared Ag/SiO$_2$ nanoaggregates (top-right inset) (adapted from ref. 296 with permission from the American Chemical Society, copyright 2021). (d) Absorption coefficient as a function of the wavelength at different Ag core sizes for a constant SiO$_2$ and Au shell thickness of 10 nm. The inset shows a multilayered Ag@SiO$_2$@Au NP with a Ag core size of 40 nm surrounded by a SiO$_2$ and Au shells. (e) Absorption coefficient as a function of the wavelength at different Au shell thicknesses for a 10 nm thick SiO$_2$ layer and Ag core size of 40 nm (adapted from ref. 298 with permission from Nature Portfolio, copyright 2019).

axis of the nanostars produced two absorption peaks but also induced a strong dipole moment in the direction of the incident light, leading to charge separation along the branches and tips of the nanostar (Fig. 13a: inset), confirming their potential for NIR-triggered drug release. In addition, 3D full-wave computational modeling showed that SiO$_2$@Au core–shell structures (Fig. 13b) and Au nano-cages exhibit higher local field enhancement compared to Au nanorods due to higher degree of rotational symmetry, making them more efficient photothermal transducers.[295] Merkl *et al.*[296] demonstrated, through a combination of UV-Vis spectra measurements and extinction spectra calculations,[297] that primarily interparticle spacing affects plasmonic coupling in flame-made Ag/SiO$_2$ nanoaggregates, rather than the constituent particle size and overall aggregate morphology. A reduction in interparticle spacing was achieved by controlling the thickness of the SiO$_2$ dielectric spacer, leading to a progressive increase in NIR extinction (Fig. 13c), highlighting the potential of these nanoaggregates as functional coatings for medical devices.

The development of materials for biomolecular detection with single-molecule sensitivity in the tissue transparent NIR region holds great promise in biomedicine. Optimizing near-field enhancement and tunable resonance in multilayered Ag@SiO$_2$@Au NPs is crucial for Raman scattering and sensing. FEM simulations[298] show that increasing the Ag core

diameter from 40 to 80 nm, shifts the absorption peak into the IR region, when maintaining the SiO$_2$ dielectric spacer and Au shell thickness at 10 nm (Fig. 13d). In contrast, decreasing the Au shell thickness from 100 to 5 nm shifts the absorption peak from red to NIR for a 40 nm Ag core (Fig. 13e), while reducing the interparticle spacing for a Ag@SiO$_2$@Au dimer maximizes the near-field enhancement.

The resonance between electron oscillations of metallic NPs (*e.g.*, Au and Pt NPs), with electromagnetic waves generates significant heat, enhancing the photothermal and thermoplasmonic properties of these materials, making them suitable for theranostics and cancer therapy applications. While Au NPs have been studied extensively,[299,300] Pt-based NPs have received little attention. Samadi *et al.*[301] investigated the thermoplasmonic properties, photothermal effects on cancer cells, and the toxicity of Pt NPs, using FEM simulations to support their experimental findings. The simulations showed that the absorption of light and irradiated temperature of Pt NPs matched the experimental data. Larger Pt NPs exhibited significantly higher irradiated temperatures and maintained structural integrity at high temperatures. Notably, the formation of a vapor layer around irradiated Pt NPs suggested potential structural changes. Simulated temperature profiles at a water/glass interface indicated that the Pt NP could become embedded in the

glass surface if vapor layers formed, with temperatures reaching around 900 °C.

Additionally, a FEM-based model was developed to predict the plasmonic resonance of Au NPs embedded in breast cancer cells.[302] By selecting appropriate factors, such as NP assembly, surrounding medium (refractive index), and inter-particle distance, the model explained experimental results, such as the higher scattering contributions of larger NPs in the optical response after light irradiation.

4 Conclusions and outlook

Nanomaterials emerge as versatile tools for biomedical applications, offering transformative possibilities from combating neurodegenerative disorders and cancers to enhancing medical equipment with antibacterial coatings and advancing biosensors. A thorough understanding of nanoparticle (NP) behavior in biological fluids and their interactions with biomolecules is essential to fully integrate them into biomedical applications and achieve clinical translation. Computational approaches facilitate the development of innovative nanomaterials by enabling exploration of NP stability, antibacterial activity, potential toxicological manifestations, and drug release rates in NP-drug systems. This review highlights the significance of computational simulations in understanding NP physicochemical characteristics, including chemical stability, oxidation, and reactivity in biofluids. Density functional theory (DFT) and molecular dynamics (MD) simulations can unravel the intricacies of nanoscale interactions that cannot be observed directly experimentally, by elucidating NP reactivity, and long-term behavior of NPs in biological media. Case studies of NP-protein interactions and drug delivery systems underscore the utility of these techniques in designing bio-compatible, functional NPs with enhanced targeting capabilities. The potential of NPs in treating neurodegenerative diseases, such as Alzheimer's and Parkinson's, is particularly compelling. Computational simulations can aid the discovery of nanomaterials tailored for these applications, the rational drug design, and the understanding of nano-biomolecular interactions.

However, force field development is pivotal for the next generation of computational nano-biomedical research. Surface NP characteristics, including crystal facets and surface chemistry, are critical to NP interactions with biological molecules. Current forcefields frequently face limitations in transferability across different systems and conditions. Furthermore, advancements in nanoparticle science and the creation of functional multicomponent nanoparticles necessitate the development of accurate forcefields. For example, doped oxides such as Co-doped iron oxide,[303] superparamagnetic iron oxide nanoparticles ($Zn_{0.5}Fe_{2.5}O_4$ and $Mn_{0.5}Fe_{2.5}O_4$) interacting with drug molecules,[304] hybrid bioglass – metal oxide nanoparticles (CeO_2 or Mn_3O_4),[305] and other nanocomposites such as SiO_2-coated TiN,[306] recently synthesized in academic laboratories show promise for appli-

cations in oral drug delivery, wound healing, and radiation therapy, highlighting this need. The reactivity and/or electromagnetic properties of these nanoparticles are also critical for their efficacy in these applications, requiring sophisticated force fields to precisely model such properties.

A second major challenge in computational biomedicine is the direct comparison between simulations and experiments, due to the different length and time scales each can accurately track. Simulations are typically limited to small nanoparticles, while experiments cannot routinely monitor the dynamics of nanoparticle–biomolecule interactions at the nanoscale. The implementation of mesoscale and multiscale simulations for modeling NP transport and NP response to external fields, can bridge the gap between experimental parameters and nanostructural characteristics, supporting the design of NPs for non-toxic drug delivery, photothermal therapy, and MRI contrast agents for biological sensing and disease diagnosis.

Although still in their early stages of development, advanced computational approaches and technologies, such as physics-informed machine learning (ML) and quantum computing, show promise for effectively bridging length and time scales in simulations. These ML models harness potential to significantly enhance the efficiency and accuracy of predictions in molecular modeling, while quantum computing can revolutionize molecular simulations by drastically accelerating computations, enabling more realistic, extensive, and sophisticated simulations. However, realizing these advancements requires fostering multidisciplinary collaborations and overcoming communication barriers across chemistry, physics, engineering, computer science, and mathematics disciplines.

Author contributions

D. C.: conceptualization, writing – original draft. E. G.: conceptualization, writing – review and editing, funding acquisition, supervision.

Data availability

No primary research results, software or code have been included and no new data were generated or analysed as part of this review.

Conflicts of interest

The authors declare no competing financial interest.

Acknowledgements

References

1 M. J. Mitchell, M. M. Billingsley, R. M. Haley, M. E. Wechsler, N. A. Peppas and R. Langer, Engineering precision nanoparticles for drug delivery, *Nat. Rev. Drug Discovery*, 2021, **20**, 101–124.

2 C. de la Encarnación, D. J. de Aberasturi and L. M. Liz-Marzán, Multifunctional plasmonic-magnetic nanoparticles for bioimaging and hyperthermia, *Adv. Drug Delivery Rev.*, 2022, 114484.

3 P. Zhang, Y. Li, W. Tang, J. Zhao, L. Jing and K. J. McHugh, Theranostic nanoparticles with disease-specific administration strategies, *Nano Today*, 2022, **42**, 101335.

4 R. Eivazzadeh-Keihan, E. Bahojb Noruzi, K. Khanmohammadi Chenab, A. Jafari, F. Radinekiyan, S. M. Hashemi, F. Ahmadpour, A. Behboudi, J. Mosafer, A. Mokhtarzadeh, *et al.*, Metal-based nanoparticles for bone tissue engineering, *J. Tissue Eng. Regener. Med.*, 2020, **14**, 1687–1714.

5 S. Duan, R. Wu, Y.-H. Xiong, H.-M. Ren, C. Lei, Y.-Q. Zhao, X.-Y. Zhang and F.-J. Xu, Multifunctional antimicrobial materials: From rational design to biomedical applications, *Prog. Mater. Sci.*, 2022, **125**, 100887.

6 G. C. Lavorato, R. Das, J. A. Masa, M.-H. Phan and H. Srikanth, Hybrid magnetic nanoparticles as efficient nanoheaters in biomedical applications, *Nanoscale Adv.*, 2021, **3**, 867–888.

7 S. Mitchell, R. Qin, N. Zheng and J. Pérez-Ramírez, Nanoscale engineering of catalytic materials for sustainable technologies, *Nat. Nanotechnol.*, 2021, **16**, 129–139.

8 L. Wang, M. Hasanzadeh Kafshgari and M. Meunier, Optical properties and applications of plasmonic-metal nanoparticles, *Adv. Funct. Mater.*, 2020, **30**, 2005400.

9 H. Haidari, N. Goswami, R. Bright, Z. Kopecki, A. J. Cowin, S. Garg and K. Vasilev, The interplay between size and valence state on the antibacterial activity of sub-10 nm silver nanoparticles, *Nanoscale Adv.*, 2019, **1**, 2365–2371.

10 J. Jeevanandam, A. Barhoum, Y. S. Chan, A. Dufresne and M. K. Danquah, Review on nanoparticles and nanostructured materials: history, sources, toxicity and regulations, *Beilstein J. Nanotechnol.*, 2018, **9**, 1050–1074.

11 L. Mädler, H. K. Kammler, R. Mueller and S. E. Pratsinis, Controlled synthesis of nanostructured particles by flame spray pyrolysis, *J. Aerosol Sci.*, 2002, **33**, 369–389.

12 R. Strobel and S. E. Pratsinis, Flame aerosol synthesis of smart nanostructured materials, *J. Mater. Chem.*, 2007, **17**, 4743–4756.

13 A. T. Güntner, N. J. Pineau and S. E. Pratsinis, Flame-made chemoresistive gas sensors and devices, *Prog. Energy Combust. Sci.*, 2022, **90**, 100992.

14 G. A. Sotiriou, D. Franco, D. Poulikakos and A. Ferrari, Optically stable biocompatible flame-made SiO_2-coated Y2O3: Tb3 + nanophosphors for cell imaging, *ACS Nano*, 2012, **6**, 3888–3897.

15 H. Schulz, B. Schimmoeller, S. E. Pratsinis, U. Salz and T. Bock, Radiopaque dental adhesives: dispersion of flame-made Ta2O5/SiO_2 nanoparticles in methacrylic matrices, *J. Dent.*, 2008, **36**, 579–587.

16 L. R. Gerken, A. Gogos, F. H. Starsich, H. David, M. E. Gerdes, H. Schiefer, S. Psoroulas, D. Meer, L. Plasswilm, D. C. Weber, *et al.*, Catalytic activity imperative for nanoparticle dose enhancement in photon and proton therapy, *Nat. Commun.*, 2022, **13**, 3248.

17 F. M. Hilty, A. Teleki, F. Krumeich, R. Büchel, R. F. Hurrell, S. E. Pratsinis and M. B. Zimmermann, Development and optimization of iron-and zinc-containing nanostructured powders for nutritional applications, *Nanotechnology*, 2009, **20**, 475101.

18 P. M. Gschwend, F. H. Starsich, R. C. Keitel and S. E. Pratsinis, Nd 3+-Doped BiVO 4 luminescent nanothermometers of high sensitivity, *Chem. Commun.*, 2019, **55**, 7147–7150.

19 D. F. Henning, P. Merkl, C. Yun, F. Iovino, L. Xie, E. Mouzourakis, C. Moularas, Y. Deligiannakis, B. Henriques-Normark, K. Leifer, *et al.*, Luminescent CeO$_2$: Eu3 + nanocrystals for robust in situ H_2O_2 real-time detection in bacterial cell cultures, *Biosens. Bioelectron.*, 2019, **132**, 286–293.

20 G. A. Sotiriou, F. Starsich, A. Dasargyri, M. C. Wurnig, F. Krumeich, A. Boss, J.-C. Leroux and S. E. Pratsinis, Photothermal killing of cancer cells by the controlled plasmonic coupling of silica-coated Au/Fe2O3 nanoaggregates, *Adv. Funct. Mater.*, 2014, **24**, 2818–2827.

21 A. T. Guntner, V. Koren, K. Chikkadi, M. Righettoni and S. E. Pratsinis, E-nose sensing of low-ppb formaldehyde in gas mixtures at high relative humidity for breath screening of lung cancer?, *ACS Sens.*, 2016, **1**, 528–535.

22 I. K. Herrmann, M. Urner, F. M. Koehler, M. Hasler, B. Roth-Z'Graggen, R. N. Grass, U. Ziegler, B. Beck-Schimmer and W. J. Stark, Blood purification using functionalized core/shell nanomagnets, *Small*, 2010, **6**, 1388–1392.

23 L.-P. Wu, D. Wang and Z. Li, Grand challenges in nanomedicine, *Mater. Sci. Eng., C*, 2020, **106**, 110302.

24 M. A. Brook, Platinum in silicone breast implants, *Biomaterials*, 2006, **27**, 3274–3286.

25 *Food and Drug Administration Backgrounder on Platinum in Silicone Breast Implants*, 2018, **https://www.fda.gov/medical-devices/breast-implants/fda-backgrounder-pl\%atinum-silicone-breast-implants**, accessed: 29.10.2024.

26 V. Harish, M. Ansari, D. Tewari, A. B. Yadav, N. Sharma, S. Bawarig, M.-L. García-Betancourt, A. Karatutlu, M. Bechelany and A. Barhoum, Cutting-edge advances in tailoring size, shape, and functionality of nanoparticles and nanostructures: A review, *J. Taiwan Inst. Chem. Eng.*, 2023, **149**, 105010.

27 Y. Kumar, A. Sinha, K. Nigam, D. Dwivedi and J. S. Sangwai, Functionalized nanoparticles: Tailoring properties through surface energetics and coordination chemistry for advanced biomedical applications, *Nanoscale*, 2023, **15**, 6075–6104.

28 S. Habib, M. Talhami, A. Hassanein, E. Mahdi, A.-E. Maryam, M. K. Hassan, A. Altaee, P. Das and A. H. Hawari, Advances in functionalization and conjugation mechanisms of dendrimers with iron oxide magnetic nanoparticles, *Nanoscale*, 2024, **16**, 13331–13372.

29 Q. Song and Z. J. Zhang, Shape control and associated magnetic properties of spinel cobalt ferrite nanocrystals, *J. Am. Chem. Soc.*, 2004, **126**, 6164–6168.

30 G. L. Nealon, B. Donnio, R. Greget, J.-P. Kappler, E. Terazzi and J.-L. Gallani, Magnetism in gold nanoparticles, *Nanoscale*, 2012, **4**, 5244–5258.

31 L. Haim, F. Robert, L. Peres, P. Lecante, K. Philippot, R. Poteau, M. Respaud and C. Amiens, Correlation between surface chemistry and magnetism in iron nanoparticles, *Nanoscale Adv.*, 2021, **3**, 4471–4481.

32 B. Rezaei, Z. Tay, S. Mostufa, O. N. Manzari, E. Azizi, S. Ciannella, C. Li, M. Zeng, J. Gomez-Pastora, K. Wu, *et al.*, Magnetic nanoparticles for magnetic particle imaging (MPI): design and applications, *Nanoscale*, 2024, **16**, 11802–11824.

33 M. D. Nguyen, L. Deng, J. M. Lee, K. M. Resendez, M. Fuller, S. Hoijang, F. Robles-Hernandez, C.-W. Chu, D. Litvinov, V. G. Hadjiev, *et al.*, Magnetic tunability via control of crystallinity and size in polycrystalline iron oxide nanoparticles, *Small*, 2024, **20**, 2402940.

34 M. Chauhan, S. M. Basu, M. Qasim and J. Giri, Polypropylene sulphide coating on magnetic nanoparticles as a novel platform for excellent biocompatible, stimuli-responsive smart magnetic nanocarriers for cancer therapeutics, *Nanoscale*, 2023, **15**, 7384–7402.

35 T. Kaur and D. Sharma, Self-propelling bacteria-based magnetic nanoparticles (BacMags) for targeted magnetic hyperthermia therapy against hypoxic tumors, *Nanoscale*, 2024, **16**, 7892–7907.

36 J. Zheng, X. Cheng, H. Zhang, X. Bai, R. Ai, L. Shao and J. Wang, Gold nanorods: the most versatile plasmonic nanoparticles, *Chem. Rev.*, 2021, **121**, 13342–13453.

37 P. Huang, P. Rong, J. Lin, W. Li, X. Yan, M. G. Zhang, L. Nie, G. Niu, J. Lu, W. Wang, *et al.*, Triphase interface synthesis of plasmonic gold bellflowers as near-infrared light mediated acoustic and thermal theranostics, *J. Am. Chem. Soc.*, 2014, **136**, 8307–8313.

38 S. M. Meyer and C. J. Murphy, Anisotropic silica coating on gold nanorods boosts their potential as SERS sensors, *Nanoscale*, 2022, **14**, 5214–5226.

39 P. Si, N. Razmi, O. Nur, S. Solanki, C. M. Pandey, R. K. Gupta, B. D. Malhotra, M. Willander and A. de la Zerda, Gold nanomaterials for optical biosensing and bioimaging, *Nanoscale Adv.*, 2021, **3**, 2679–2698.

40 A. Arbuz, A. Sultangaziyev, A. Rapikov, Z. Kunushpayeva and R. Bukasov, How gap distance between gold nano-particles in dimers and trimers on metallic and non-metallic SERS substrates can impact signal enhancement, *Nanoscale Adv.*, 2022, **4**, 268–280.

41 G. Pasparakis, Recent developments in the use of gold and silver nanoparticles in biomedicine, *Wiley Interdiscip. Rev.:Nanomed. Nanobiotechnol.*, 2022, **14**, e1817.

42 X. Chen and H. J. Schluesener, Nanosilver: a nanoproduct in medical application, *Toxicol. Lett.*, 2008, **176**, 1–12.

43 G. A. Sotiriou, A. Meyer, J. T. Knijnenburg, S. Panke and S. E. Pratsinis, Quantifying the origin of released Ag+ ions from nanosilver, *Langmuir*, 2012, **28**, 15929–15936.

44 S. Tang and J. Zheng, Antibacterial activity of silver nanoparticles: structural effects, *Adv. Healthcare Mater.*, 2018, **7**, 1701503.

45 A. Menichetti, A. Mavridi-Printezi, D. Mordini and M. Montalti, Effect of Size, Shape and Surface Functionalization on the Antibacterial Activity of Silver Nanoparticles, *J. Funct. Biomater.*, 2023, **14**, 244.

46 S. Nikolova, M. Milusheva, V. Gledacheva, M. Feizi-Dehnayebi, L. Kaynarova, D. Georgieva, V. Delchev, I. Stefanova, Y. Tumbarski, R. Mihaylova, *et al.*, Drug-Delivery Silver Nanoparticles: A New Perspective for Phenindione as an Anticoagulant, *Biomedicines*, 2023, **11**, 2201.

47 A. Alkaladi, A. M. Abdelazim and M. Afifi, Antidiabetic activity of zinc oxide and silver nanoparticles on streptozotocin-induced diabetic rats, *Int. J. Mol. Sci.*, 2014, **15**, 2015–2023.

48 H. Lin, A. BoLatai and N. Wu, Application progress of nano silver dressing in the treatment of diabetic foot, *Diabetes, Metab. Syndr. Obes.*, 2021, 4145–4154.

49 K. Manivannan, C.-C. Cheng, R. Anbazhagan, H.-C. Tsai and J.-K. Chen, Fabrication of silver seeds and nanoparticle on core-shell Ag@ SiO$_2$ nanohybrids for combined photothermal therapy and bioimaging, *J. Colloid Interface Sci.*, 2019, **537**, 604–614.

50 W. Xie, P. Qiu and C. Mao, Bio-imaging, detection and analysis by using nanostructures as SERS substrates, *J. Mater. Chem.*, 2011, **21**, 5190–5202.

51 C. Caro, P. Quaresma, E. Pereira, J. Franco, M. Pernia Leal, M. L. García-Martín, J. L. Royo, J. M. Oliva-Montero, P. J. Merkling, A. P. Zaderenko, *et al.*, Synthesis and characterization of elongated-shaped silver nanoparticles as a biocompatible anisotropic SERS probe for intracellular imaging: theoretical modeling and experimental verification, *Nanomaterials*, 2019, **9**, 256.

52 M. Potara, S. Boca, E. Licarete, A. Damert, M.-C. Alupei, M. T. Chiriac, O. Popescu, U. Schmidt and S. Astilean, Chitosan-coated triangular silver nanoparticles as a novel class of biocompatible, highly sensitive plasmonic platforms for intracellular SERS sensing and imaging, *Nanoscale*, 2013, **5**, 6013–6022.

53 A. A. Yaqoob, K. Umar and M. N. M. Ibrahim, Silver nanoparticles: various methods of synthesis, size affecting factors and their potential applications–a review, *Appl. Nanosci.*, 2020, **10**, 1369–1378.

54 A. Anwar, K. Rajendran, R. Siddiqui, M. Raza Shah and N. A. Khan, Clinically approved drugs against CNS diseases as potential therapeutic agents to target brain-eating amoebae, *ACS Chem. Neurosci.*, 2018, **10**, 658–666.

55 A. K. Suresh, D. A. Pelletier, W. Wang, J. L. Morrell-Falvey, B. Gu and M. J. Doktycz, Cytotoxicity induced by engineered silver nanocrystallites is dependent on surface coatings and cell types, *Langmuir*, 2012, **28**, 2727–2735.

56 S. Vijayakumar, B. Vaseeharan, B. Malaikozhundan, N. Gopi, P. Ekambaram, R. Pachaiappan, P. Velusamy, K. Murugan, G. Benelli, R. S. Kumar, *et al.*, Therapeutic effects of gold nanoparticles synthesized using Musa paradisiaca peel extract against multiple antibiotic resistant Enterococcus faecalis biofilms and human lung cancer cells (A549), *Microb. Pathog.*, 2017, **102**, 173–183.

57 P. Joshi, S. Chakraborti, J. E. Ramirez-Vick, Z. Ansari, V. Shanker, P. Chakrabarti and S. P. Singh, The anticancer activity of chloroquine-gold nanoparticles against MCF-7 breast cancer cells, *Colloids Surf., B*, 2012, **95**, 195–200.

58 J. Lee, D. K. Chatterjee, M. H. Lee and S. Krishnan, Gold nanoparticles in breast cancer treatment: promise and potential pitfalls, *Cancer Lett.*, 2014, **347**, 46–53.

59 M. Ganeshkumar, M. Sathishkumar, T. Ponrasu, M. G. Dinesh and L. Suguna, Spontaneous ultra fast synthesis of gold nanoparticles using Punica granatum for cancer targeted drug delivery, *Colloids Surf., B*, 2013, **106**, 208–216.

60 S. Kunjiappan, C. Bhattacharjee and R. Chowdhury, In vitro antioxidant and hepatoprotective potential of Azolla microphylla phytochemically synthesized gold nanoparticles on acetaminophen–induced hepatocyte damage in Cyprinus carpio L., *In Vitro Cell. Dev. Biol.: Anim.*, 2015, **51**, 630–643.

61 S. Sivanesan and S. Rajeshkumar, Gold nanoparticles in diagnosis and treatment of alzheimer's disease, *Nanobiotechnol. Neurodegener. Dis.*, 2019, 289–306.

62 C. Kohout, C. Santi and L. Polito, Anisotropic gold nanoparticles in biomedical applications, *Int. J. Mol. Sci.*, 2018, **19**, 3385.

63 D.-Z. Lin, P.-C. Chuang, P.-C. Liao, J.-P. Chen and Y.-F. Chen, Increasing the spectral shifts in LSPR biosensing using DNA-functionalized gold nanorods in a competitive assay format for the detection of interferon-γ, *Biosens. Bioelectron.*, 2016, **81**, 221–228.

64 K. Nejati, M. Dadashpour, T. Gharibi, H. Mellatyar and A. Akbarzadeh, Biomedical applications of functionalized gold nanoparticles: a review, *J. Cluster Sci.*, 2021, 1–16.

65 C.-C. Wang, S.-M. Wu, H.-W. Li and H.-T. Chang, Biomedical Applications of DNA-Conjugated Gold Nanoparticles, *ChemBioChem*, 2016, **17**, 1052–1062.

66 A. M. Al-Enizi, T. Ahamad, A. B. Al-Hajji, J. Ahmed, A. A. Chaudhary and S. M. Alshehri, Cellulose gum and copper nanoparticles based hydrogel as antimicrobial agents against urinary tract infection (UTI) pathogens, *Int. J. Biol. Macromol.*, 2018, **109**, 803–809.

67 L. Song, M. Connolly, M. L. Fernández-Cruz, M. G. Vijver, M. Fernández, E. Conde, G. R. de Snoo, W. J. Peijnenburg and J. M. Navas, Species-specific toxicity of copper nanoparticles among mammalian and piscine cell lines, *Nanotoxicology*, 2014, **8**, 383–393.

68 S. A. Ghoto, M. Y. Khuhawar, T. M. Jahangir and J. u. D. Mangi, Applications of copper nanoparticles for colorimetric detection of dithiocarbamate pesticides, *J. Nanostruct. Chem.*, 2019, **9**, 77–93.

69 W. Zheng, L. Hu, L. Y. S. Lee and K.-Y. Wong, Copper nanoparticles/polyaniline/graphene composite as a highly sensitive electrochemical glucose sensor, *J. Electroanal. Chem.*, 2016, **781**, 155–160.

70 A. Chwalibog, E. Sawosz, A. Hotowy, J. Szeliga, S. Mitura, K. Mitura, M. Grodzik, P. Orlowski and A. Sokolowska, Visualization of interaction between inorganic nanoparticles and bacteria or fungi, *Int. J. Nanomed.*, 2010, 1085–1094.

71 M. Jeyaraj, S. Gurunathan, M. Qasim, M.-H. Kang and J.-H. Kim, A comprehensive review on the synthesis, characterization, and biomedical application of platinum nanoparticles, *Nanomaterials*, 2019, **9**, 1719.

72 S. B. Subramaniyan, A. Ramani, V. Ganapathy and V. Anbazhagan, Preparation of self-assembled platinum nanoclusters to combat Salmonella typhi infection and inhibit biofilm formation, *Colloids Surf., B*, 2018, **171**, 75–84.

73 A. A. Pawar, J. Sahoo, A. Verma, A. Lodh and J. Lakkakula, Usage of platinum nanoparticles for anticancer therapy over last decade: a review, *Part. Part. Syst. Charact.*, 2021, **38**, 2100115.

74 M. Kutwin, E. Sawosz, S. Jaworski, M. Wierzbicki, B. Strojny, M. Grodzik, M. Ewa Sosnowska, M. Trzaskowski and A. Chwalibog, Nanocomplexes of graphene oxide and platinum nanoparticles against colorectal cancer Colo205, HT-29, HTC-116, SW480, liver cancer HepG2, human breast cancer MCF-7, and adenocarcinoma LNCaP and human cervical Hela B cell lines, *Materials*, 2019, **12**, 909.

75 T. T. Loan, L. T. Do and H. Yoo, Platinum nanoparticles induce apoptosis on raw 264.7 macrophage cells, *J. Nanosci. Nanotechnol.*, 2018, **18**, 861–864.

76 X. Yang, D. Salado-Leza, E. Porcel, C. R. González-Vargas, F. Savina, D. Dragoe, H. Remita and S. Lacombe, A facile one-pot synthesis of versatile PEGylated platinum nanoflowers and their application in radiation therapy, *Int. J. Mol. Sci.*, 2020, **21**, 1619.

77 D. Pedone, M. Moglianetti, E. De Luca, G. Bardi and P. P. Pompa, Platinum nanoparticles in nanobiomedicine, *Chem. Soc. Rev.*, 2017, **46**, 4951–4975.

78 M. Moglianetti, E. De Luca, D. Pedone, R. Marotta, T. Catelani, B. Sartori, H. Amenitsch, S. F. Retta and P. P. Pompa, Platinum nanozymes recover cellular ROS homeostasis in an oxidative stress-mediated disease model, *Nanoscale*, 2016, **8**, 3739–3752.

79 P. Velmurugan, J. Shim, K. Kim and B.-T. Oh, Prunus × yedoensis tree gum mediated synthesis of platinum nanoparticles with antifungal activity against phytopathogens, *Mater. Lett.*, 2016, **174**, 61–65.

80 D. Chen, C. Zhao, J. Ye, Q. Li, X. Liu, M. Su, H. Jiang, C. Amatore, M. Selke and X. Wang, In situ biosynthesis of fluorescent platinum nanoclusters: toward self-bioimaging-guided cancer theranostics, *ACS Appl. Mater. Interfaces*, 2015, **7**, 18163–18169.

81 Q. Cheng and Y. Liu, Multifunctional platinum-based nanoparticles for biomedical applications, *Wiley Interdiscip. Rev.: Nanomed. Nanobiotechnol.*, 2017, **9**, e1410.

82 M. Rafi, H. Cabral, M. Kano, P. Mi, C. Iwata, M. Yashiro, K. Hirakawa, K. Miyazono, N. Nishiyama and K. Kataoka, Polymeric micelles incorporating (1, 2-diaminocyclohexane) platinum(II) suppress the growth of orthotopic scirrhous gastric tumors and their lymph node metastasis, *J. Controlled Release*, 2012, **159**, 189–196.

83 C. Streich, L. Akkari, C. Decker, J. Bormann, C. Rehbock, A. Muller-Schiffmann, F. C. Niemeyer, L. Nagel-Steger, D. Willbold, B. Sacca, *et al.*, Characterizing the effect of multivalent conjugates composed of Aβ-specific ligands and metal nanoparticles on neurotoxic fibrillar aggregation, *ACS Nano*, 2016, **10**, 7582–7597.

84 Y.-B. Miao, H.-X. Ren, Q. Zhong and F.-X. Song, Tailoring a luminescent metal- organic framework precise inclusion of Pt-Aptamer nanoparticle for noninvasive monitoring Parkinson's disease, *Chem. Eng. J.*, 2022, **441**, 136009.

85 J. Nellore, C. Pauline and K. Amarnath, Bacopa monnieri phytochemicals mediated synthesis of platinum nanoparticles and its neurorescue effect on 1-methyl 4-phenyl 1, 2, 3, 6 tetrahydropyridine-induced experimental parkinsonism in zebrafish, *J. Neurodegener. Dis.*, 2013, **2013**, 1–8.

86 N. Behera, M. Arakha, M. Priyadarshinee, B. S. Pattanayak, S. Soren, S. Jha and B. C. Mallick, Oxidative stress generated at nickel oxide nanoparticle interface results in bacterial membrane damage leading to cell death, *RSC Adv.*, 2019, **9**, 24888–24894.

87 Q. Wang, Y.-F. Xu, G.-L. Xu, H. Su, S.-Y. Shen, T.-T. Tu, L. Huang, J.-T. Li and S.-G. Sun, Synthesis of hierarchical NiO microsphere with waxberry-like structure and its enhanced lithium storage performance, *J. Alloys Compd.*, 2015, **648**, 59–66.

88 J. Iqbal, B. A. Abbasi, R. Ahmad, M. Mahmoodi, A. Munir, S. A. Zahra, A. Shahbaz, M. Shaukat, S. Kanwal, S. Uddin, *et al.*, Phytogenic synthesis of nickel oxide nanoparticles (NiO) using fresh leaves extract of Rhamnus triquetra (wall.) and investigation of its multiple in vitro biological potentials, *Biomedicines*, 2020, **8**, 117.

89 A. H. Hashem, M. A. Al Abboud, M. M. Alawlaqi, T. M. Abdelghany and M. Hasanin, Synthesis of nanocapsules based on biosynthesized nickel nanoparticles and potato starch: Antimicrobial, antioxidant, and anticancer activity, *Starch/Staerke*, 2022, **74**, 2100165.

90 H. Chen, Z. Mei, K. Qi, Y. Wang and R. Chen, A wearable enzyme-free glucose sensor based on nickel nanoparticles decorated laser-induced graphene, *J. Electroanal. Chem.*, 2022, **920**, 116585.

91 E. Velasco, V. G. Baldovino-Medrano, E. M. Gaigneaux and S. A. Giraldo, Development of an efficient strategy for coating tio 2 on polyester–cotton fabrics for bactericidal applications, *Top. Catal.*, 2016, **59**, 378–386.

92 A. Mansoor, Z. Khurshid, M. T. Khan, E. Mansoor, F. A. Butt, A. Jamal and P. J. Palma, Medical and dental applications of titania nanoparticles: an overview, *Nanomaterials*, 2022, **12**, 3670.

93 S. Sargazi, E. Simge, S. S. Gelen, A. Rahdar, M. Bilal, R. Arshad, N. Ajalli, M. F. A. Khan and S. Pandey, Application of titanium dioxide nanoparticles in photothermal and photodynamic therapy of cancer: An updated and comprehensive review, *J. Drug Delivery Sci. Technol.*, 2022, 103605.

94 D. G. You, V. Deepagan, W. Um, S. Jeon, S. Son, H. Chang, H. I. Yoon, Y. W. Cho, M. Swierczewska, S. Lee, *et al.*, ROS-generating TiO2 nanoparticles for non-invasive sonodynamic therapy of cancer, *Sci. Rep.*, 2016, **6**, 23200.

95 M. Pourmadadi, M. Rajabzadeh-Khosroshahi, M. M. Eshaghi, E. Rahmani, H. Motasadizadeh, R. Arshad, A. Rahdar and S. Pandey, TiO2-based nanocomposites for cancer diagnosis and therapy: a comprehensive review, *J. Drug Delivery Sci. Technol.*, 2023, **82**, 104370.

96 S. Liang, X. Deng, G. Xu, X. Xiao, M. Wang, X. Guo, P. Ma, Z. Cheng, D. Zhang and J. Lin, A novel Pt–TiO2 heterostructure with oxygen-deficient layer as bilaterally enhanced sonosensitizer for synergistic chemo-sono-dynamic cancer therapy, *Adv. Funct. Mater.*, 2020, **30**, 1908598.

97 M. W. Akram, F. Raziq, M. Fakhar-e-Alam, M. H. Aziz, K. Alimgeer, M. Atif, M. Amir, A. Hanif and W. A. Farooq, Tailoring of Au-TiO2 nanoparticles conjugated with doxorubicin for their synergistic response and photodynamic therapy applications, *J. Photochem. Photobiol., A*, 2019, **384**, 112040.

98 K. Xu, L. Jin, L. Xu, Y. Zhu, L. Hong, C. Pan, Y. Li, J. Yao, R. Zou, W. Tang, *et al.*, IGF1 receptor-targeted black TiO2 nanoprobes for MRI-guided synergetic photothermal-chemotherapy in drug resistant pancreatic tumor, *J. Nanobiotechnol.*, 2022, **20**, 1–17.

99 R. M. Patil, N. D. Thorat, P. B. Shete, P. A. Bedge, S. Gavde, M. G. Joshi, S. A. Tofail and R. A. Bohara, Comprehensive cytotoxicity studies of superparamagnetic iron oxide nanoparticles, *Biochem. Biophys. Rep.*, 2018, **13**, 63–72.

100 M. Mahmoudi, M. A. Shokrgozar, A. Simchi, M. Imani, A. S. Milani, P. Stroeve, H. Vali, U. O. Hafeli and S. Bonakdar, Multiphysics flow modeling and in vitro toxicity of iron oxide nanoparticles coated with poly (vinyl alcohol), *J. Phys. Chem. C*, 2009, **113**, 2322–2331.

101 K. Velsankar, G. Parvathy, S. Mohandoss, G. Ravi and S. Sudhahar, Echinochloa frumentacea grains extract

mediated synthesis and characterization of iron oxide nanoparticles: A greener nano drug for potential biomedical applications, *J. Drug Delivery Sci. Technol.*, 2022, **76**, 103799.

102 L. Gloag, M. Mehdipour, D. Chen, R. D. Tilley and J. J. Gooding, Advances in the application of magnetic nanoparticles for sensing, *Adv. Mater.*, 2019, **31**, 1904385.

103 D. Y. Lee, S. Kang, Y. Lee, J. Y. Kim, D. Yoo, W. Jung, S. Lee, Y. Y. Jeong, K. Lee and S. Jon, PEGylated bilirubin-coated iron oxide nanoparticles as a biosensor for magnetic relaxation switching-based ROS detection in whole blood, *Theranostics*, 2020, **10**, 1997.

104 D. Stanicki, T. Vangijzegem, I. Ternad and S. Laurent, An update on the applications and characteristics of magnetic iron oxide nanoparticles for drug delivery, *Expert Opin. Drug Delivery*, 2022, **19**, 321–335.

105 N. P. Truong, M. R. Whittaker, C. W. Mak and T. P. Davis, The importance of nanoparticle shape in cancer drug delivery, *Expert Opin. Drug Delivery*, 2015, **12**, 129–142.

106 R. P. Friedrich, I. Cicha and C. Alexiou, Iron oxide nanoparticles in regenerative medicine and tissue engineering, *Nanomaterials*, 2021, **11**, 2337.

107 A. Curcio, A. K. Silva, S. Cabana, A. Espinosa, B. Baptiste, N. Menguy, C. Wilhelm and A. Abou-Hassan, Iron oxide nanoflowers@ CuS hybrids for cancer tri-therapy: interplay of photothermal therapy, magnetic hyperthermia and photodynamic therapy, *Theranostics*, 2019, **9**, 1288.

108 M. Khan, Z.-u.-R. Mashwani, M. Ikram, N. I. Raja, A. H. Mohamed, G. Ren and A. A. Omar, Efficacy of green cerium oxide nanoparticles for potential therapeutic applications: Circumstantial insight on mechanistic aspects, *Nanomaterials*, 2022, **12**, 2117.

109 S. Pansambal, R. Oza, S. Borgave, A. Chauhan, P. Bardapurkar, S. Vyas and S. Ghotekar, Bioengineered cerium oxide (CeO$_2$) nanoparticles and their diverse applications: a review, *Appl. Nanosci.*, 2022, 1–26.

110 K. R. Singh, V. Nayak, T. Sarkar and R. P. Singh, Cerium oxide nanoparticles: properties, biosynthesis and biomedical application, *RSC Adv.*, 2020, **10**, 27194–27214.

111 N. Pourkhalili, A. Hosseini, A. Nili-Ahmadabadi, S. Hassani, M. Pakzad, M. Baeeri, A. Mohammadirad and M. Abdollahi, Biochemical and cellular evidence of the benefit of a combination of cerium oxide nanoparticles and selenium to diabetic rats, *World J. Diabetes*, 2011, **2**, 204.

112 Q. Maqbool, M. Nazar, S. Naz, T. Hussain, N. Jabeen, R. Kausar, S. Anwaar, F. Abbas and T. Jan, Antimicrobial potential of green synthesized CeO$_2$ nanoparticles from Olea europaea leaf extract, *Int. J. Nanomed.*, 2016, 5015–5025.

113 R. Gao, R. N. Mitra, M. Zheng, K. Wang, J. C. Dahringer and Z. Han, Developing Nanoceria-Based pH-Dependent Cancer-Directed Drug Delivery System for Retinoblastoma, *Adv. Funct. Mater.*, 2018, **28**, 1806248.

114 I.-A. Turin-Moleavin, A. Fifere, A.-L. Lungoci, I. Rosca, A. Coroaba, D. Peptanariu, V. Nastasa, S.-A. Pasca, A.-C. Bostanaru, M. Mares, *et al.*, In vitro and in vivo anti-oxidant activity of the new magnetic-cerium oxide nano-conjugates, *Nanomaterials*, 2019, **9**, 1565.

115 Z. Zand, P. A. Khaki, A. Salihi, M. Sharifi, N. M. Qadir Nanakali, A. A. Alasady, F. M. Aziz, K. Shahpasand, A. Hasan and M. Falahati, Cerium oxide NPs mitigate the amyloid formation of α-synuclein and associated cytotoxicity, *Int. J. Nanomed.*, 2019, 6989–7000.

116 T. Naganuma and E. Traversa, The effect of cerium valence states at cerium oxide nanoparticle surfaces on cell proliferation, *Biomaterials*, 2014, **35**, 4441–4453.

117 J. Dolai, K. Mandal and N. R. Jana, Nanoparticle size effects in biomedical applications, *ACS Appl. Nano Mater.*, 2021, **4**, 6471–6496.

118 P. Chhour, J. Kim, B. Benardo, A. Tovar, S. Mian, H. I. Litt, V. A. Ferrari and D. P. Cormode, Effect of gold nanoparticle size and coating on labeling monocytes for CT tracking, *Bioconjugate Chem.*, 2017, **28**, 260–269.

119 C. P. Joshi and T. P. Bigioni, Model for the phase transfer of nanoparticles using ionic surfactants, *Langmuir*, 2014, **30**, 13837–13843.

120 X. Wan, X. Zhang, W. Pan, B. Liu, L. Yu, H. Wang, N. Li and B. Tang, Ratiometric fluorescent quantification of the size-dependent cellular toxicity of silica nanoparticles, *Anal. Chem.*, 2019, **91**, 6088–6096.

121 L. Yang, Z. Zhou, J. Song and X. Chen, Anisotropic nanomaterials for shape-dependent physicochemical and biomedical applications, *Chem. Soc. Rev.*, 2019, **48**, 5140–5176.

122 X. Zhang, P. Zheng, Y. Ma, Y. Jiang and H. Li, Atomic-scale understanding of oxidation mechanisms of materials by computational approaches: A review, *Mater. Des.*, 2022, **217**, 110605.

123 P. Grammatikopoulos, M. Sowwan and J. Kioseoglou, Computational modeling of nanoparticle coalescence, *Adv. Theory Simul.*, 2019, **2**, 1900013.

124 T. Pfeiffer, A. De Nicola, C. Montis, F. Carla, N. F. van der Vegt, D. Berti and G. Milano, Nanoparticles at biomimetic interfaces: combined experimental and simulation study on charged gold nanoparticles/lipid bilayer interfaces, *J. Phys. Chem. Lett.*, 2018, **10**, 129–137.

125 I. Rouse, D. Power, E. G. Brandt, M. Schneemilch, K. Kotsis, N. Quirke, A. P. Lyubartsev and V. Lobaskin, First principles characterisation of bio–nano interface, *Phys. Chem. Chem. Phys.*, 2021, **23**, 13473–13482.

126 V. Lobaskin, J. Subbotina and I. Rouse, Computational modelling of bionano interface, *Europhys. Lett.*, 2023, **143**, 57001.

127 M. Ray, G. Brancolini, D. C. Luther, Z. Jiang, R. Cao-Milán, A. M. Cuadros, A. Burden, V. Clark, S. Rana, R. Mout, *et al.*, High affinity protein surface binding through co-engineering of nanoparticles and proteins, *Nanoscale*, 2022, **14**, 2411–2418.

128 M. A. Nguyen, Z. E. Hughes, Y. Liu, Y. Li, M. T. Swihart, M. R. Knecht and T. R. Walsh, Peptide-mediated growth and dispersion of Au nanoparticles in water via sequence engineering, *J. Phys. Chem. C*, 2018, **122**, 11532–11542.

129 G. Brancolini, L. Bellucci, M. C. Maschio, R. Di Felice and S. Corni, The interaction of peptides and proteins with nanostructures surfaces: a challenge for nanoscience, *Curr. Opin. Colloid Interface Sci.*, 2019, **41**, 86–94.

130 M. Penna, K. Ley, S. Maclaughlin and I. Yarovsky, Surface heterogeneity: a friend or foe of protein adsorption–insights from theoretical simulations, *Faraday Discuss.*, 2016, **191**, 435–464.

131 A. De Nicola, S. Hezaveh, Y. Zhao, T. Kawakatsu, D. Roccatano and G. Milano, Micellar drug nanocarriers and biomembranes: how do they interact?, *Phys. Chem. Chem. Phys.*, 2014, **16**, 5093–5105.

132 G. Rossi, S. Salassi, F. Simonelli, A. Bartocci and L. Monticelli, Nanoparticle–Membrane Interactions: Surface Effects, *Biomembr. Simul.*, 2019, 163–176.

133 P. Charchar, A. J. Christofferson, N. Todorova and I. Yarovsky, Understanding and designing the gold–bio interface: Insights from simulations, *Small*, 2016, **12**, 2395–2418.

134 B. B. Noble, N. Todorova and I. Yarovsky, Electromagnetic bioeffects: a multiscale molecular simulation perspective, *Phys. Chem. Chem. Phys.*, 2022, **24**, 6327–6348.

135 T. Saliev, Z. Mustapova, G. Kulsharova, D. Bulanin and S. Mikhalovsky, Therapeutic potential of electromagnetic fields for tissue engineering and wound healing, *Cell Proliferation*, 2014, **47**, 485–493.

136 L. Li, X. Guo, X. Peng, H. Zhang, Y. Liu, H. Li, X. He, D. Shi, B. Xiong, Y. Zhao, *et al.*, Radiofrequency-responsive dual-valent gold nanoclusters for enhancing synergistic therapy of tumor ablation and artery embolization, *Nano Today*, 2020, **35**, 100934.

137 M. Khademalrasool and M. D. Talebzadeh, Rapid synthesis of silver nanowires during the polyol-microwave method and COMSOL multiphysics simulation of electromagnetic heating, *Adv. Powder Technol.*, 2021, **32**, 2916–2928.

138 S. Manrique-Bedoya, M. Abdul-Moqueet, P. Lopez, T. Gray, M. Disiena, A. Locker, S. Kwee, L. Tang, R. L. Hood, Y. Feng, *et al.*, Multiphysics modeling of plasmonic photothermal heating effects in gold nanoparticles and nanoparticle arrays, *J. Phys. Chem. C*, 2020, **124**, 17172–17182.

139 F. A. Del Castillo, N. T. Emerson and H. Yang, Evaluating the Accuracy of the COMSOL-Based Finite-Element Method for Simulating Plasmon-Modified Fluorescence, *J. Phys. Chem. B*, 2024, **128**, 10789–10798.

140 E. G. Karvelas, N. Lampropoulos, L. Benos, T. Karakasidis and I. E. Sarris, On the magnetic aggregation of Fe3O4 nanoparticles, *Comput. Methods Programs Biomed.*, 2021, **198**, 105778.

141 D. D. Li, X. Gu, V. Timchenko, Q. N. Chan, A. C. Yuen and G. H. Yeoh, Study of morphology and optical properties of gold nanoparticle aggregates under different pH conditions, *Langmuir*, 2018, **34**, 10340–10352.

142 I. N. Levine, D. H. Busch and H. Shull, *Quantum chemistry*, Pearson Prentice Hall Upper Saddle River, NJ, 2009, vol. 6.

143 W. Koch and M. C. Holthausen, *A chemist's guide to density functional theory*, John Wiley & Sons, 2015.

144 L. Goerigk, A. Hansen, C. Bauer, S. Ehrlich, A. Najibi and S. Grimme, A look at the density functional theory zoo with the advanced GMTKN55 database for general main group thermochemistry, kinetics and noncovalent interactions, *Phys. Chem. Chem. Phys.*, 2017, **19**, 32184–32215.

145 L. Goerigk and N. Mehta, A trip to the density functional theory zoo: warnings and recommendations for the user, *Aust. J. Chem.*, 2019, **72**, 563–573.

146 L. Kuster, M. Bélanger-Bouliga, T. E. Shaw, A. Nazemi, M. Frenette, *et al.*, Insight into the nature of carbon–metal bonding for N-heterocyclic carbenes in gold/silver complexes and nanoparticles using DFT-correlated Raman spectroscopy: strong evidence for π-backbonding, *Nanoscale*, 2024, **16**, 11052–11068.

147 A. Fakharnezhad, D. M. Saad, G. A. Kelesidis and E. Goudeli, Nucleation Rate of Soot by n-Heptane Pyrolysis, *Aerosol Sci. Technol.*, 2025, DOI: **10.1080/ 02786826.2025.2480625**.

148 A. Sharma, K. M. Mukut, S. P. Roy and E. Goudeli, The coalescence of incipient soot clusters, *Carbon*, 2021, **180**, 215–225.

149 B. Buesser, A. Grohn and S. E. Pratsinis, Sintering rate and mechanism of TiO2 nanoparticles by molecular dynamics, *J. Phys. Chem. C*, 2011, **115**, 11030–11035.

150 Y. Wang and E. Goudeli, The onset of aerosol Au nanoparticle crystallization: accretion & explosive nucleation, *Nanoscale*, 2024, **16**, 17942–17953.

151 B. Hong and A. Z. Panagiotopoulos, Molecular dynamics simulations of silica nanoparticles grafted with poly(ethylene oxide) oligomer chains, *J. Phys. Chem. C*, 2012, **116**, 2385–2395.

152 X. Wang, R. Lei, L. Li, X. Fei, R. Ju, X. Sun, H. Cao, Q. Zhang, C. Chen and X. Wang, Rearrangement of protein structures on a gold nanoparticle surface is regulated by ligand adsorption modes, *Nanoscale*, 2021, **13**, 20425–20436.

153 T. P. Senftle, S. Hong, M. M. Islam, S. B. Kylasa, Y. Zheng, Y. K. Shin, C. Junkermeier, R. Engel-Herbert, M. J. Janik, H. M. Aktulga, *et al.*, The ReaxFF reactive force-field: development, applications and future directions, *npj Comput. Mater.*, 2016, **2**, 1–14.

154 T. Liang, T.-R. Shan, Y.-T. Cheng, B. D. Devine, M. Noordhoek, Y. Li, Z. Lu, S. R. Phillpot and S. B. Sinnott, Classical atomistic simulations of surfaces and heterogeneous interfaces with the charge-optimized many body (COMB) potentials, *Mater. Sci. Eng., R*, 2013, **74**, 255–279.

155 S. Chernousova and M. Epple, Silver as antibacterial agent: ion, nanoparticle, and metal, *Angew. Chem., Int. Ed.*, 2013, **52**, 1636–1653.

156 A. Nene, M. Galluzzi, L. Hongrong, P. Somani, S. Ramakrishna and X.-F. Yu, Synthetic preparations and atomic scale engineering of silver nanoparticles for biomedical applications, *Nanoscale*, 2021, **13**, 13923–13942.

157 J. Liu and R. H. Hurt, Ion release kinetics and particle persistence in aqueous nano-silver colloids, *Environ. Sci Technol.*, 2010, **44**, 2169–2175.

158 A. C. Quevedo, I. Lynch and E. Valsami-Jones, Silver nanoparticle induced toxicity and cell death mechanisms in embryonic zebrafish cells, *Nanoscale*, 2021, **13**, 6142–6161.

159 B. E. Erickson, Nanosilver pesticides, *Chem. Eng. News*, 2009, **87**, 25–26.

160 J. Pal, T. B. Rawal, M. Smerieri, S. Hong, M. Alatalo, L. Savio, L. Vattuone, T. S. Rahman and M. Rocca, Adatom Extraction from pristine metal terraces by dissociative oxygen adsorption: Combined STM and density functional theory investigation of O/Ag (110), *Phys. Rev. Lett.*, 2017, **118**, 226101.

161 D. Chaparro and E. Goudeli, Oxidation Rate and Crystallinity Dynamics of Silver Nanoparticles at High Temperatures, *J. Phys. Chem. C*, 2023, **127**, 13389–13397.

162 D. Chaparro and E. Goudeli, Shape-dependent oxidation rates of nano-structured silver particles, *J. Chem. Phys.*, 2024, **161**, 124704–124708.

163 M. Li, M. T. Curnan, M. A. Gresh-Sill, S. D. House, W. A. Saidi and J. C. Yang, Unusual layer-by-layer growth of epitaxial oxide islands during Cu oxidation, *Nat. Commun.*, 2021, **12**, 2781.

164 M. H. Almarzoug, D. Ali, S. Alarifi, S. Alkahtani and A. M. Alhadheq, Platinum nanoparticles induced genotoxicity and apoptotic activity in human normal and cancer hepatic cells via oxidative stress-mediated Bax/Bcl-2 and caspase-3 expression, *Environ. Toxicol.*, 2020, **35**, 930–941.

165 P. Asharani, N. Xinyi, M. P. Hande and S. Valiyaveettil, DNA damage and p53-mediated growth arrest in human cells treated with platinum nanoparticles, *Nanomedicine*, 2010, **5**, 51–64.

166 A. A. Alshatwi, J. Athinarayanan and P. Vaiyapuri Subbarayan, Green synthesis of platinum nanoparticles that induce cell death and G2/M-phase cell cycle arrest in human cervical cancer cells, *J. Mater. Sci.: Mater. Med.*, 2015, **26**, 1–9.

167 Y. Yamagishi, A. Watari, Y. Hayata, X. Li, M. Kondoh, Y. Yoshioka, Y. Tsutsumi and K. Yagi, Acute and chronic nephrotoxicity of platinum nanoparticles in mice, *Nanoscale Res. Lett.*, 2013, **8**, 1–7.

168 T. Yin, Z. Wang, X. Li, Y. Li, K. Bian, W. Cao, Y. He, H. Liu, K. Niu and D. Gao, Biologically inspired self-assembly of bacitracin-based platinum nanoparticles with anti-tumor effects, *New J. Chem.*, 2017, **41**, 2941–2948.

169 C.-T. Chien, J.-Y. Yan, W.-C. Chiu, T.-H. Wu, C.-Y. Liu and S.-Y. Lin, Caged Pt nanoclusters exhibiting corrodibility to exert tumor-inside activation for anticancer chemotherapeutics, *Adv. Mater.*, 2013, **25**, 5067–5073.

170 R. Slapikas, I. Dabo and S. B. Sinnott, Surface reconstruction of oxidized platinum nanoparticles using classical molecular dynamics simulations, *Comput. Mater. Sci.*, 2022, **209**, 111364.

171 Y. Han, R. Lupitskyy, T.-M. Chou, C. M. Stafford, H. Du and S. Sukhishvili, Effect of oxidation on surface-enhanced Raman scattering activity of silver nanoparticles: a quantitative correlation, *Anal. Chem.*, 2011, **83**, 5873–5880.

172 J. S. Hong, J. Pyun, Y. W. Park, C. S. Kim and I.-B. Shim, Oxidation effect in cobalt nanoparticles Magnetic Fluids, *IEEE Trans. Magn.*, 2009, **45**, 2464–2466.

173 B. Farkaš, D. Santos-Carballal, A. Cadi-Essadek and N. H. De Leeuw, A DFT+ U study of the oxidation of cobalt nanoparticles: Implications for biomedical applications, *Materialia*, 2019, **7**, 100381.

174 Q. Sun, A. Kandalam, Q. Wang, P. Jena, Y. Kawazoe and M. Marquez, Effect of Au coating on the magnetic and structural properties of Fe nanoclusters for use in biomedical applications: A density-functional theory study, *Phys. Rev. B:Condens. Matter Mater. Phys.*, 2006, **73**, 134409.

175 S. M. Day, D. Duquaine, L. V. Mundada, R. G. Menon, B. V. Khan, S. Rajagopalan and W. P. Fay, Chronic iron administration increases vascular oxidative stress and accelerates arterial thrombosis, *Circulation*, 2003, **107**, 2601–2606.

176 R. Jinnouchi, K. K. T. Suzuki and Y. Morimoto, DFT calculations on electro-oxidations and dissolutions of Pt and Pt–Au nanoparticles, *Catal. Today*, 2016, **262**, 100–109.

177 B. Farkaš and N. H. de Leeuw, AuCo nanoparticles: ordering, magnetisation, and morphology trends predicted by DFT, *Phys. Chem. Chem. Phys.*, 2022, **24**, 10451–10464.

178 N. Eom, M. E. Messing, J. Johansson and K. Deppert, Sintering mechanism of core@ shell metal@ metal oxide nanoparticles, *J. Phys. Chem. C*, 2021, **125**, 16220–16227.

179 M. Capdevila-Cortada and N. López, Entropic contributions enhance polarity compensation for CeO$_2$ (100) surfaces, *Nat. Mater.*, 2017, **16**, 328–334.

180 D. Selli, G. Fazio and C. Di Valentin, Modelling realistic TiO2 nanospheres: A benchmark study of SCC-DFTB against hybrid DFT, *J. Chem. Phys.*, 2017, **147**, 164701–164712.

181 L. Steinmetz, C. Geers, S. Balog, M. Bonmarin, L. Rodriguez-Lorenzo, P. Taladriz-Blanco, B. Rothen-Rutishauser and A. Petri-Fink, A comparative study of silver nanoparticle dissolution under physiological conditions, *Nanoscale Adv.*, 2020, **2**, 5760–5768.

182 R. E. Slapikas, I. Dabo and S. B. Sinnott, Atomic-scale modeling of the dissolution of oxidized platinum nanoparticles in an explicit water environment, *J. Mater. Chem. A*, 2023, **11**, 7043–7052.

183 J. L. Fajin, M. N. D. S. Cordeiro and J. R. Gomes, Density functional theory study of the water dissociation on platinum surfaces: General trends, *J. Phys. Chem. A*, 2014, **118**, 5832–5840.

184 J. L. Fajín, M. N. D. Cordeiro and J. R. Gomes, On the theoretical understanding of the unexpected O 2 activation by nanoporous gold, *Chem. Commun.*, 2011, **47**, 8403–8405.

185 F. Grote and A. P. Lyubartsev, Water structure, dynamics and reactivity on a TiO 2-nanoparticle surface: new insights from ab initio molecular dynamics, *Nanoscale*, 2022, **14**, 16536–16547.

186 Z. Futera and N. J. English, Exploring rutile (110) and anatase (101) TiO2 water interfaces by reactive force-field simulations, *J. Phys. Chem. C*, 2017, **121**, 6701–6711.

187 T. X. Sayle, M. Molinari, S. Das, U. M. Bhatta, G. Möbus, S. C. Parker, S. Seal and D. C. Sayle, Environment-mediated structure, surface redox activity and reactivity of ceria nanoparticles, *Nanoscale*, 2013, **5**, 6063–6073.

188 A. Kazemi-Beydokhti, S. Zeinali Heris and M. Jaafari, Experimental investigation of thermal conductivity of medical nanofluids based on functionalised single-wall carbon nanotube and conjugated cisplatin, *Micro Nano Lett.*, 2015, **10**, 241–247.

189 Q. Wu, H. Zhang, M. Chen, Y. Zhang, J. Huang, Z. Xu and W. Wang, Preparation of carbon-coated iron nanofluid and its application in radiofrequency ablation, *J. Biomed. Mater. Res., Part B*, 2015, **103**, 908–914.

190 N. S. Akbar, A. W. Butt and D. Tripathi, Biomechanically driven unsteady non-uniform flow of copper water and Silver water nanofluids through finite length channel, *Comput. Methods Programs Biomed.*, 2017, **146**, 1–9.

191 N. Sher Akbar, E. Maraj and S. Nadeem, Copper nanoparticle analysis for peristaltic flow in a curved channel with heat transfer characteristics, *Eur. Phys. J. Plus*, 2014, **129**, 1–11.

192 I. H. El-Sayed, X. Huang and M. A. El-Sayed, Surface plasmon resonance scattering and absorption of anti-EGFR antibody conjugated gold nanoparticles in cancer diagnostics: applications in oral cancer, *Nano Lett.*, 2005, **5**, 829–834.

193 E. Guisasola, A. Baeza, L. Asín, J. M. de la Fuente and M. Vallet-Regí, Heating at the Nanoscale through Drug-Delivery Devices: Fabrication and Synergic Effects in Cancer Treatment with Nanoparticles, *Small Methods*, 2018, **2**, 1800007.

194 S. F. Noraldeen, L. Jin and L. Zhou, Size, interface and temperature effects on specific heat capacities of Cu-water nanofluid and Cu nanoparticle: A molecular analysis, *Therm. Sci. Eng. Prog.*, 2022, **27**, 101157.

195 E. V. Timofeeva, J. L. Routbort and D. Singh, Particle shape effects on thermophysical properties of alumina nanofluids, *J. Appl. Phys.*, 2009, **106**, 014304–014310.

196 Y. Zhai, Y. Li, Z. Xuan, Z. Li and H. Wang, Determination of heat transport mechanism using nanoparticle property and interfacial nanolayer in a nanofluidic system, *J. Mol. Liq.*, 2021, **344**, 117787.

197 Y. Jiang, S. Dehghan, A. Karimipour, D. Toghraie, Z. Li and I. Tlili, Effect of copper nanoparticles on thermal behavior of water flow in a zig-zag nanochannel using molecular dynamics simulation, *Int. Commun. Heat Mass Transfer*, 2020, **116**, 104652.

198 Y. Shang, R. B. Dehkordi, S. Chupradit, D. Toghraie, A. Sevbitov, M. Hekmatifar, W. Suksatan and R. Sabetvand, The computational study of microchannel thickness effects on H₂O/CuO nanofluid flow with molecular dynamics simulations, *J. Mol. Liq.*, 2022, **345**, 118240.

199 R. B. Dehkordi, D. Toghraie, M. Hashemian, F. Aghadavoudi and M. Akbari, Molecular dynamics simulation of ferro-nanofluid flow in a microchannel in the presence of external electric field: Effects of Fe3O4 nanoparticles, *Int. Commun. Heat Mass Transfer*, 2020, **116**, 104653.

200 M. Farzinpour, D. Toghraie, B. Mehmandoust, F. Aghadavoudi and A. Karimipour, Molecular dynamics study of barrier effects on Ferro-nanofluid flow in the presence of constant and time-dependent external magnetic fields, *J. Mol. Liq.*, 2020, **308**, 113152.

201 P. Martin, P. Zhang, P. M. Rodger and E. Valsami-Jones, Simulations of morphological transformation in silver nanoparticles as a tool for assessing their reactivity and potential toxicity, *NanoImpact*, 2019, **14**, 100147.

202 D. A. Walker, E. K. Leitsch, R. J. Nap, I. Szleifer and B. A. Grzybowski, Geometric curvature controls the chemical patchiness and self-assembly of nanoparticles, *Nat. Nanotechnol.*, 2013, **8**, 676–681.

203 R. Razavi, M. Amiri, H. A. Alshamsi, T. Eslaminejad and M. Salavati-Niasari, Green synthesis of Ag nanoparticles in oil-in-water nano-emulsion and evaluation of their anti-bacterial and cytotoxic properties as well as molecular docking, *Arabian J. Chem.*, 2021, **14**, 103323.

204 S. K. Verma, E. Jha, P. K. Panda, A. Thirumurugan, S. Patro, S. Parashar and M. Suar, Molecular insights to alkaline based bio-fabrication of silver nanoparticles for inverse cytotoxicity and enhanced antibacterial activity, *Mater. Sci. Eng., C*, 2018, **92**, 807–818.

205 Y. Chen, L. Ren, L. Sun, X. Bai, G. Zhuang, B. Cao, G. Hu, N. Zheng and S. Liu, Amphiphilic silver nanoclusters show active nano–bio interaction with compelling antibacterial activity against multidrug-resistant bacteria, *NPG Asia Mater.*, 2020, **12**, 56.

206 M. Arakha, S. M. Borah, M. Saleem, A. N. Jha and S. Jha, Interfacial assembly at silver nanoparticle enhances the antibacterial efficacy of nisin, *Free Radicals Biol. Med.*, 2016, **101**, 434–445.

207 C. Tang, D. Hu, Q. Cao, W. Yan and B. Xing, Silver nanoparticles-loaded activated carbon fibers using chitosan as binding agent: Preparation, mechanism, and their antibacterial activity, *Appl. Surf. Sci.*, 2017, **394**, 457–465.

208 S. Sinha and D. Vohora, Drug discovery and development: An overview, *Pharm. Med. Transl. Clin. Res.*, 2018, 19–32.

209 B. McLean and I. Yarovsky, Structure, Properties, and Applications of Silica Nanoparticles: Recent Theoretical Modeling Advances, Challenges, and Future Directions, *Small*, 2024, 2405299.

210 P. G. T. Perera, N. Todorova, Z. Vilagosh, O. Bazaka, K. Bazaka, R. J. Crawford, R. J. Croft, I. Yarovsky, E. P. Ivanova, *et al.*, Translocation of silica nanospheres through giant unilamellar vesicles (GUVs) induced by a

high frequency electromagnetic field, *RSC Adv.*, 2021, **11**, 31408–31420.

211 M. Penna, K. J. Ley, A. Belessiotis-Richards, S. MacLaughlin, D. A. Winkler and I. Yarovsky, Hydration and dynamics of ligands determine the antifouling capacity of functionalized surfaces, *J. Phys. Chem. C*, 2019, **123**, 30360–30372.

212 M. Penna and I. Yarovsky, Nanoscale in silico classification of ligand functionalised surfaces for protein adsorption resistance, *Nanoscale*, 2020, **12**, 7240–7255.

213 H. Lopez and V. Lobaskin, Coarse-grained model of adsorption of blood plasma proteins onto nanoparticles, *J. Chem. Phys.*, 2015, **143**, 243138.

214 R. Gupta, Y. Badhe, S. Mitragotri and B. Rai, Permeation of nanoparticles across the intestinal lipid membrane: dependence on shape and surface chemistry studied through molecular simulations, *Nanoscale*, 2020, **12**, 6318–6333.

215 X. Lin, X. Lin and N. Gu, Optimization of hydrophobic nanoparticles to better target lipid rafts with molecular dynamics simulations, *Nanoscale*, 2020, **12**, 4101–4109.

216 F. Neri, A. Scala, S. Grimato, M. Santoro, S. Spadaro, F. Barreca, F. Cimino, A. Speciale, A. Saija, G. Grassi, *et al.*, Biocompatible silver nanoparticles embedded in a PEG–PLA polymeric matrix for stimulated laser light drug release, *J. Nanopart. Res.*, 2016, **18**, 1–14.

217 M. C. R. Miranda, N. C. Sato, G. S. P. Brasil, R. D. Piazza, M. Jafelicci, N. R. de Barros, F. A. Borges, A. Batagin-Neto, W. de Melo Silva, R. D. Herculano, *et al.*, Silver nanoparticles effect on drug release of metronidazole in natural rubber latex dressing, *Polym. Bull.*, 2021, 1–17.

218 T. Ngake, M. Gulumian, S. Cronjé and R. Harris, Modelling and simulation study of the influence of size and surface functionality on the stability of PEG-functionalised AgNPs, *Mol. Simul.*, 2023, **49**, 197–207.

219 R. Harris, The PEGylated and non-PEGylated interaction of the anticancer drug 5-fluorouracil with paramagnetic Fe3O4 nanoparticles as drug carrier, *J. Mol. Liq.*, 2022, **360**, 119515.

220 J. Subbotina, I. Rouse and V. Lobaskin, In silico prediction of protein binding affinities onto core–shell PEGylated noble metal nanoparticles for rational design of drug nanocarriers, *Nanoscale*, 2023, **15**, 13371–13383.

221 J. Subbotina and V. Lobaskin, Multiscale modeling of bio-nano interactions of zero-valent silver nanoparticles, *J. Phys. Chem. B*, 2022, **126**, 1301–1314.

222 S. A. Alsharif, D. Power, I. Rouse and V. Lobaskin, In silico prediction of protein adsorption energy on titanium dioxide and gold nanoparticles, *Nanomaterials*, 2020, **10**, 1967.

223 B. Khodashenas, M. Ardjmand, M. S. Baei, A. S. Rad and A. A. Khiyavi, Gelatin–gold nanoparticles as an ideal candidate for curcumin drug delivery: experimental and DFT studies, *J. Inorg. Organomet. Polym. Mater.*, 2019, **29**, 2186–2196.

224 B. Khodashenas, M. Ardjmand, M. S. Baei, A. S. Rad and A. Akbarzadeh, Conjugation of pectin biopolymer with Au-nanoparticles as a drug delivery system: Experimental and DFT studies, *Appl. Organomet. Chem.*, 2020, **34**, e5609.

225 R. Anthony Harris, H. van der Walt and P. Morgan Shumbula, Engineered inorganic/organic-core/shell magnetic FexOy nanoparticles with oleic acid and/or oleylamine as capping agents, *Curr. Pharm. Des.*, 2015, **21**, 5369–5388.

226 L. Dai Tran, B. H. Nguyen, N. Van Hieu, H. V. Tran, H. Le Nguyen and P. X. Nguyen, Electrochemical detection of short HIV sequences on chitosan/Fe3O4 nanoparticle based screen printed electrodes, *Mater. Sci. Eng., C*, 2011, **31**, 477–485.

227 L. Qiang, Z. Li, T. Zhao, S. Zhong, H. Wang and X. Cui, Atomic-scale interactions of the interface between chitosan and Fe3O4, *Colloids Surf., A*, 2013, **419**, 125–132.

228 S. Yu, A. Perálvarez-Marín, C. Minelli, J. Faraudo, A. Roig and A. Laromaine, Albumin-coated SPIONs: An experimental and theoretical evaluation of protein conformation, binding affinity and competition with serum proteins, *Nanoscale*, 2016, **8**, 14393–14405.

229 R. Harris, Chemotherapy drug temozolomide adsorbed onto iron-oxide (Fe3O4) nanoparticles as nanocarrier: A simulation study, *J. Mol. Liq.*, 2019, **288**, 111084.

230 S. Shirazi-Fard, F. Mohammadpour, A. R. Zolghadr and A. Klein, Encapsulation and release of doxorubicin from TiO2 nanotubes: Experiment, density functional theory calculations, and molecular dynamics simulation, *J. Phys. Chem. B*, 2021, **125**, 5549–5558.

231 T. Ashwini, R. Narayan, P. A. Shenoy and U. Y. Nayak, Computational modeling for the design and development of nano based drug delivery systems, *J. Mol. Liq.*, 2022, 120596.

232 R. Morad, M. Akbari, P. Rezaee, A. Koochaki, M. Maaza and Z. Jamshidi, First principle simulation of coated hydroxychloroquine on Ag, Au and Pt nanoparticles, *Sci. Rep.*, 2021, **11**, 2131.

233 Y. Hou, X. Dan, M. Babbar, Y. Wei, S. G. Hasselbalch, D. L. Croteau and V. A. Bohr, Ageing as a risk factor for neurodegenerative disease, *Nat. Rev. Neurol.*, 2019, **15**, 565–581.

234 G. Marucci, M. Buccioni, D. Dal Ben, C. Lambertucci, R. Volpini and F. Amenta, Efficacy of acetylcholinesterase inhibitors in Alzheimer's disease, *Neuropharmacology*, 2021, **190**, 108352.

235 D. Chaparro, A. Flores-Gaspar and J. Alí-Torres, Computational design of copper ligands with controlled metal chelating, pharmacokinetics, and redox properties for Alzheimer's disease, *J. Alzheimer's Dis.*, 2021, **82**, S179–S193.

236 N. Puentes-Díaz, D. Chaparro, D. Morales-Morales, A. Flores-Gaspar and J. Alí-Torres, Role of metal cations of copper, Iron, and aluminum and multifunctional ligands in Alzheimer's disease: experimental and computational insights, *ACS Omega*, 2023, **8**, 4508–4526.

237 N. Puentes-Díaz, D. Chaparro, V. Reyes-Marquez, D. Morales-Morales, A. Flores-Gaspar and J. Alí-Torres,

Computational Evaluation of the Potential Pharmacological Activity of Salen-Type Ligands in Alzheimer's Disease, *J. Alzheimer's Dis.*, 2023, 1–14.

238 S. M. Asil, J. Ahlawat, G. G. Barroso and M. Narayan, Nanomaterial based drug delivery systems for the treatment of neurodegenerative diseases, *Biomater. Sci.*, 2020, **8**, 4109–4128.

239 F. Tavanti, A. Pedone and M. C. Menziani, Disclosing the Interaction of Gold Nanoparticles with Aβ (1–40) Monomers through Replica Exchange Molecular Dynamics Simulations, *Int. J. Mol. Sci.*, 2020, **22**, 26.

240 W. Lin, T. Insley, M. D. Tuttle, L. Zhu, D. A. Berthold, P. Kral, C. M. Rienstra and C. J. Murphy, Control of protein orientation on gold nanoparticles, *J. Phys. Chem. C*, 2015, **119**, 21035–21043.

241 W. Zhang, A. J. Christofferson, Q. A. Besford, J. J. Richardson, J. Guo, Y. Ju, K. Kempe, I. Yarovsky and F. Caruso, Metal-dependent inhibition of amyloid fibril formation: synergistic effects of cobalt–tannic acid networks, *Nanoscale*, 2019, **11**, 1921–1928.

242 M. Z. Pedram, A. Shamloo, A. Alasty and E. Ghafar-Zadeh, Toward epileptic brain region detection based on magnetic nanoparticle patterning, *Sensors*, 2015, **15**, 24409–24427.

243 M. Lazaratos, K. Karathanou, E. Mainas, A. Chatzigoulas, N. Pippa, C. Demetzos and Z. Cournia, Coating of magnetic nanoparticles affects their interactions with model cell membranes, *Biochim. Biophys. Acta, Gen. Subj.*, 2020, **1864**, 129671.

244 M. Z. Pedram, A. Shamloo, A. Alasty and E. Ghafar-Zadeh, Optimal magnetic field for crossing super-para-magnetic nanoparticles through the brain blood barrier: a computational approach, *Biosensors*, 2016, **6**, 25.

245 R. A. Harris, Simulation study on the physicochemical properties of Fe3O4 nanoparticles as drug delivery vehicles for dopamine replacement therapy of Parkinson's disease, *Mater. Today Commun.*, 2022, **31**, 103829.

246 P. Sarker, M. S. J. Sajib, X. Tao and T. Wei, Multiscale simulation of protein corona formation on silver nanoparticles: study of ovispirin-1 peptide adsorption, *J. Phys. Chem. B*, 2022, **126**, 601–608.

247 D. Power, I. Rouse, S. Poggio, E. Brandt, H. Lopez, A. Lyubartsev and V. Lobaskin, A multiscale model of protein adsorption on a nanoparticle surface, *Modell. Simul. Mater. Sci. Eng.*, 2019, **27**, 084003.

248 I. Rouse and V. Lobaskin, A hard-sphere model of protein corona formation on spherical and cylindrical nanoparticles, *Biophys. J.*, 2021, **120**, 4457–4471.

249 H. Chou, C. Wu, F. Lin and J. Rick, Interactions between silver nanoparticles and polyvinyl alcohol nanofibers, *AIP Adv.*, 2014, **4**, 087111–087120.

250 F. Simonelli, G. Rossi and L. Monticelli, Role of ligand conformation on nanoparticle–protein interactions, *J. Phys. Chem. B*, 2019, **123**, 1764–1769.

251 G. Brosio, G. Rossi and D. Bochicchio, Nanoparticle-induced biomembrane fusion: unraveling the effect of core size on stalk formation, *Nanoscale Adv.*, 2023, **5**, 4675–4680.

252 E. Canepa, S. Salassi, A. L. de Marco, C. Lambruschini, D. Odino, D. Bochicchio, F. Canepa, C. Canale, S. Dante, R. Brescia, *et al.*, Amphiphilic gold nanoparticles perturb phase separation in multidomain lipid membranes, *Nanoscale*, 2020, **12**, 19746–19759.

253 E. Lavagna, J. Barnoud, G. Rossi and L. Monticelli, Size-dependent aggregation of hydrophobic nanoparticles in lipid membranes, *Nanoscale*, 2020, **12**, 9452–9461.

254 E. Lavagna, D. Bochicchio, A. L. De Marco, Z. P. Güven, F. Stellacci and G. Rossi, Ion-bridges and lipids drive aggregation of same-charge nanoparticles on lipid membranes, *Nanoscale*, 2022, **14**, 6912–6921.

255 H. Ahmed, H. Lopez, F. Boselli, G. Tarricone, S. Vercellino, P. E. Costantini, V. Castagnola, M. Veronesi, F. Benfenati, A. Danielli, *et al.*, Biomimetic Plasmonic Nanophages by Head/Tail Self-Assembling: Gold Nanoparticle/Virus Interactions, *ACS Nano*, 2024, **18**, 21302–21315.

256 D. O. Idisi, C. C. Ahia, E. L. Meyer and E. M. Benecha, Effect of microstrain on the magnetic properties of reduced graphene oxide by Fe3O4 nanoparticles: insight from experimental and density functional theory, *Appl. Phys. A*, 2023, **129**, 227.

257 S. M. Thomas, H. Zhang, K. Wang, M. R. Knecht and T. R. Walsh, Exploiting Materials Binding Peptides for the Organization of Resilient Biomolecular Constructs, *Biomacromolecules*, 2024, **25**, 7216–7224.

258 M. Hamzeh and G. I. Sunahara, In vitro cytotoxicity and genotoxicity studies of titanium dioxide (TiO2) nanoparticles in Chinese hamster lung fibroblast cells, *Toxicol. in Vitro*, 2013, **27**, 864–873.

259 M. Shakeel, F. Jabeen, S. Shabbir, M. S. Asghar, M. S. Khan and A. S. Chaudhry, Toxicity of nano-titanium dioxide (TiO 2-NP) through various routes of exposure: a review, *Biol. Trace Elem. Res.*, 2016, **172**, 1–36.

260 S. Y. Fam, C. F. Chee, C. Y. Yong, K. L. Ho, A. R. Mariatulqabtiah and W. S. Tan, Stealth coating of nanoparticles in drug-delivery systems, *Nanomaterials*, 2020, **10**, 787.

261 E. Donadoni, P. Siani, G. Frigerio, C. Milani, Q. Cui and C. Di Valentin, Effect of polymer coating on nanoparticles interaction with lipid membranes by coarse-grained molecular dynamics simulations, *Nanoscale*, 2024, **16**, 9108–9122.

262 X. Shen, Z. Wang, X. Gao and Y. Zhao, Density functional theory-based method to predict the activities of nanomaterials as peroxidase mimics, *ACS Catal.*, 2020, **10**, 12657–12665.

263 A. Kyrychenko, O. M. Korsun, I. I. Gubin, S. M. Kovalenko and O. N. Kalugin, Atomistic simulations of coating of silver nanoparticles with poly (vinylpyrrolidone) oligomers: Effect of oligomer chain length, *J. Phys. Chem. C*, 2015, **119**, 7888–7899.

264 A. Lahouari, J.-P. Piquemal and J. Richardi, ReaxFF Simulations of Self-Assembled Monolayers on Silver

Surfaces and Nanocrystals, *J. Phys. Chem. C*, 2024, **128**, 1193–1201.

265 M. Zúñiga-Bustos, J. Comer and H. Poblete, Thermodynamics of the physisorption of capping agents on silver nanoparticles, *Phys. Chem. Chem. Phys.*, 2023, **25**, 20320–20330.

266 N. Baildya, I. Dey, A. Bagchi and A. P. Chattopadhyay, Interaction of copper nanoparticles with DNA: structural and docking studies, *J. Biomol. Struct. Dyn.*, 2020, **38**, 1256–1261.

267 F. Simonelli, D. Bochicchio, R. Ferrando and G. Rossi, Monolayer-protected anionic Au nanoparticles walk into lipid membranes step by step, *J. Phys. Chem. Lett.*, 2015, **6**, 3175–3179.

268 M. Das, U. Dahal, O. Mesele, D. Liang and Q. Cui, Molecular dynamics simulation of interaction between functionalized nanoparticles with lipid membranes: Analysis of coarse-grained models, *J. Phys. Chem. B*, 2019, **123**, 10547–10561.

269 T. Yamanaka, A. De Nicola, G. Munaò, T. A. Soares and G. Milano, Effect of the ligand's bulkiness on the shape of functionalized gold nanoparticles in aqueous solutions: A molecular dynamics study, *Chem. Phys. Lett.*, 2019, **731**, 136576.

270 S. Dey, R. Rivas-Barbosa, F. Sciortino, E. Zaccarelli and P. Zijlstra, Biomolecular interactions on densely coated nanoparticles: a single-molecule perspective, *Nanoscale*, 2024, **16**, 4872–4879.

271 J. H. Soh, Y. Lin, M. R. Thomas, N. Todorova, C. Kallepitis, I. Yarovsky, J. Y. Ying and M. M. Stevens, Distinct bimodal roles of aromatic molecules in controlling gold nanorod growth for biosensing, *Adv. Funct. Mater.*, 2017, **27**, 1700523.

272 S. C. Brooks, R. Jin, V. C. Zerbach, Y. Zhang, T. R. Walsh and N. L. Rosi, Single amino acid modifications for controlling the helicity of peptide-based chiral gold nanoparticle superstructures, *J. Am. Chem. Soc.*, 2023, **145**, 6546–6553.

273 T. Tarjányi, F. Bogár, J. Minárovits, M. Gajdács and Z. Tóth, Interaction of biomolecules with anatase, rutile and amorphous TiO2 surfaces: A molecular dynamics study, *PLoS One*, 2023, **18**, e0289467.

274 S. Motta, P. Siani, E. Donadoni, G. Frigerio, L. Bonati and C. Di Valentin, Metadynamics simulations for the investigation of drug loading on functionalized inorganic nanoparticles, *Nanoscale*, 2023, **15**, 7909–7919.

275 E. Donadoni, G. Frigerio, P. Siani, S. Motta, J. Vertemara, L. De Gioia, L. Bonati and C. Di Valentin, Molecular Dynamics for the Optimal Design of Functionalized Nanodevices to Target Folate Receptors on Tumor Cells, *ACS Biomater. Sci. Eng.*, 2023, **9**, 6123–6137.

276 M. Ivanov and A. P. Lyubartsev, Atomistic molecular dynamics simulations of lipids near TiO2 nanosurfaces, *J. Phys. Chem. B*, 2021, **125**, 8048–8059.

277 E. Goudeli and S. E. Pratsinis, Gas-phase manufacturing of nanoparticles: molecular dynamics and mesoscale simulations, *Part. Sci. Technol.*, 2016, **34**, 483–493.

278 E. Goudeli, M. L. Eggersdorfer and S. E. Pratsinis, Coagulation of agglomerates consisting of polydisperse primary particles, *Langmuir*, 2016, **32**, 9276–9285.

279 M. L. Eggersdorfer and E. Goudeli, Structure and dynamics of fractal-like particles made by agglomeration and sintering, *AIChE J.*, 2020, **66**, e17099.

280 A. Spyrogianni, K. S. Karadima, E. Goudeli, V. G. Mavrantzas and S. E. Pratsinis, Mobility and settling rate of agglomerates of polydisperse nanoparticles, *J. Chem. Phys.*, 2018, **148**, 064703–064718.

281 J. M. Cohen, G. M. DeLoid and P. Demokritou, A critical review of in vitro dosimetry for engineered nanomaterials, *Nanomedicine*, 2015, **10**, 3015–3032.

282 G. Mancardi, M. Alberghini, N. Aguilera-Porta, M. Calatayud, P. Asinari and E. Chiavazzo, Multi-scale modelling of aggregation of TiO2 nanoparticle suspensions in water, *Nanomaterials*, 2022, **12**, 217.

283 M. Baalousha, G. Cornelis, T. Kuhlbusch, I. Lynch, C. Nickel, W. Peijnenburg and N. Van Den Brink, Modeling nanomaterial fate and uptake in the environment: current knowledge and future trends, *Environ. Sci.: Nano*, 2016, **3**, 323–345.

284 R. Saidur, K. Leong and H. A. Mohammed, A review on applications and challenges of nanofluids, *Renewable Sustainable Energy Rev.*, 2011, **15**, 1646–1668.

285 R. Liu, H. H. Liu, Z. Ji, C. H. Chang, T. Xia, A. E. Nel and Y. Cohen, Evaluation of toxicity ranking for metal oxide nanoparticles via an in vitro dosimetry model, *ACS Nano*, 2015, **9**, 9303–9313.

286 P. M. Hinderliter, K. R. Minard, G. Orr, W. B. Chrisler, B. D. Thrall, J. G. Pounds and J. G. Teeguarden, ISDD: A computational model of particle sedimentation, diffusion and target cell dosimetry for in vitro toxicity studies, *Part. Fibre Toxicol.*, 2010, **7**, 1–20.

287 Q. Ma, J. Young, J. Gao, Y. Tao and W. Zhang, Nanoscale hydrophobicity and electrochemical mapping provides insights into facet dependent silver nanoparticle dissolution, *J. Phys. Chem. Lett.*, 2023, **14**, 2665–2673.

288 A. Al-Zubeidi, F. Stein, C. Flatebo, C. Rehbock, S. A. Hosseini Jebeli, C. F. Landes, S. Barcikowski and S. Link, Single-particle hyperspectral imaging reveals kinetics of silver ion leaching from alloy nanoparticles, *ACS Nano*, 2021, **15**, 8363–8375.

289 W. Brullot, V. K. Valev and T. Verbiest, Magnetic-plasmonic nanoparticles for the life sciences: calculated optical properties of hybrid structures, *Nanomedicine*, 2012, **8**, 559–568.

290 A. F. Bakuzis, L. C. Branquinho, L. L. e Castro, M. T. A. e Eloi and R. Miotto, Chain formation and aging process in biocompatible polydisperse ferrofluids: Experimental investigation and Monte Carlo simulations, *Adv. Colloid Interface Sci.*, 2013, **191**, 1–21.

291 L. M. Roa-Barrantes and D. J. Rodriguez Patarroyo, Magnetic field effect on the magnetic nanoparticles trajectories in pulsating blood flow: a computational model, *BioNanoScience*, 2022, **12**, 571–581.

292 A. Egel, L. Pattelli, G. Mazzamuto, D. S. Wiersma and U. Lemmer, CELES: CUDA-accelerated simulation of electromagnetic scattering by large ensembles of spheres, *J. Quant. Spectrosc. Radiat. Transfer*, 2017, **199**, 103–110.

293 A. Egel, K. M. Czajkowski, D. Theobald, K. Ladutenko, A. S. Kuznetsov and L. Pattelli, SMUTHI: A python package for the simulation of light scattering by multiple particles near or between planar interfaces, *J. Quant. Spectrosc. Radiat. Transfer*, 2021, **273**, 107846.

294 A. Tomitaka, H. Arami, A. Ahmadivand, N. Pala, A. J. McGoron, Y. Takemura, M. Febo and M. Nair, Magneto-plasmonic nanostars for image-guided and NIR-triggered drug delivery, *Sci. Rep.*, 2020, **10**, 10115.

295 K. Liu, X. Xue and E. P. Furlani, Theoretical comparison of optical properties of near-infrared colloidal plasmonic nanoparticles, *Sci. Rep.*, 2016, **6**, 34189.

296 P. Merkl, S. Zhou, A. Zaganiaris, M. Shahata, A. Eleftheraki, T. Thersleff and G. A. Sotiriou, Plasmonic coupling in silver nanoparticle aggregates and their polymer composite films for near-infrared photothermal biofilm eradication, *ACS Appl. Nano Mater.*, 2021, **4**, 5330–5339.

297 B. Auguié, J. L. Alonso-Gómez, A. Guerrero-Martínez and L. M. Liz-Marzán, Fingers crossed: Optical activity of a chiral dimer of plasmonic nanorods, *J. Phys. Chem. Lett.*, 2011, **2**, 846–851.

298 D. Paria, C. Zhang and I. Barman, Towards rational design and optimization of near-field enhancement and spectral tunability of hybrid core-shell plasmonic nanoprobes, *Sci. Rep.*, 2019, **9**, 16071.

299 S. A. Bansal, V. Kumar, J. Karimi, A. P. Singh and S. Kumar, Role of gold nanoparticles in advanced biomedical applications, *Nanoscale Adv.*, 2020, **2**, 3764–3787.

300 C. I. Giunta, S. A. Nazemi, M. Olesińska and P. Shahgaldian, Plasmonic photothermal activation of an organosilica shielded cold-adapted lipase co-immobilised with gold nanoparticles on silica particles, *Nanoscale Adv.*, 2023, **5**, 81–87.

301 A. Samadi, H. Klingberg, L. Jauffred, A. Kjær, P. M. Bendix and L. B. Oddershede, Platinum nanoparticles: a non-toxic, effective and thermally stable alternative plasmonic material for cancer therapy and bioengineering, *Nanoscale*, 2018, **10**, 9097–9107.

302 M. P. Ogáyar, R. López-Méndez, I. Figueruelo-Campanero, T. Muñoz-Ortiz, C. Wilhelm, D. Jaque, A. Espinosa and A. Serrano, Finite element modeling of plasmonic resonances in photothermal gold nanoparticles embedded in cells, *Nanoscale Adv.*, 2024, **6**, 4635–4646.

303 K. Venkatesan, D. Rajan Babu, M. P. Kavya Bai, R. Supriya, R. Vidya, S. Madeswaran, P. Anandan, M. Arivanandhan and Y. Hayakawa, Structural and magnetic properties of cobalt-doped iron oxide nanoparticles prepared by solution combustion method for biomedical applications, *Int. J. Nanomed.*, 2015, **10**, 189–198.

304 S. R. Ansari, N.-J. Hempel, S. Asad, P. Svedlindh, C. A. Bergstrom, K. Lobmann and A. Teleki, Hyperthermia-induced in situ drug amorphization by superparamagnetic nanoparticles in oral dosage forms, *ACS Appl. Mater. Interfaces*, 2022, **14**, 21978–21988.

305 R. Nißler, L. Dennebouy, A. Gogos, L. R. Gerken, M. Dommke, M. Zimmermann, M. A. Pais, A. L. Neuer, M. T. Matter, V. M. Kissling, *et al.*, Protein Aggregation on Metal Oxides Governs Catalytic Activity and Cellular Uptake, *Small*, 2024, **20**, 2311115.

306 P. M. Gschwend, S. Conti, A. Kaech, C. Maake and S. E. Pratsinis, Silica-coated TiN particles for killing cancer cells, *ACS Appl. Mater. Interfaces*, 2019, **11**, 22550–22560.